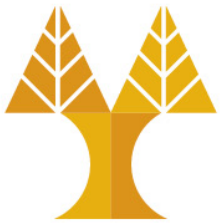

University of Cyprus
Department of Physics

Extracting Nucleon Generalized Form Factors using Lattice QCD simulations

Author:
Maria Elena Panagiotou

Supervisor:
Prof. Constantia Alexandrou

A thesis submitted in partial fulfillment of the requirements for the
Bachelor of Science Degree in Physics
May 2025

Abstract

The study of the nuclear properties holds a crucial role to understanding the fundamental properties of strong interactions. Using simulation methods for Lattice QCD gives us the advantage of researching these properties, discarding any experimental limitation we would otherwise have. In this work we calculate two nuclear GFFs, A_{20} and B_{20}, which contribute to the nucleon spin, J, and average momentum fraction. We use three $N_f = 2 + 1 + 1$ ensembles, generated by the Extended Twisted Mass Collaboration (ETMC), with three different lattice spacings to compute these quantities and extrapolate to the continuum limit.

Acknowledgements

First and foremost, I would like to express my gratitude towards Prof. Constantia Alexandrou, who has trusted me to work on such an interesting project. Her guidance and support throughout this work was beyond comparable. I have to give my sincere respect towards Dr. Yan Li and Luis Chacon. They were always open to have discussions, enlightening me with their knowledge. Their help has been of great value regarding my introduction to the subject and the accomplishment of this work.

I am deeply grateful to my family, for always supporting me and encouraging me to follow the path that leads to self-fulfillment, even when it gets tough along the way. To my friends, I am immensely thankful for always being by my side, comforting and being there for me, no matter the circumstances.

Last but not least, I must express my deep love to the five people who have made this journey more enjoyable. They have managed to bring their sweet flavors to dull moments, taking away the sorrow and pain, and for that, I feel blessed to have met them and to have them in my life. The memories we have created together are carved deep into my heart.

Contents

1 Introduction

1.1 The Standard Model

There are four fundamental forces acting in the universe: the electromagnetic (EM), weak and strong interactions and the gravitational force. The Standard Model (SM), one of the most remarkable works of late 20^{th} century, marks the first attempt to combine all of them in one theory of interacting fields. It is based on the work of Glashow[1], who combined the electromagnetic and weak interactions in 1961, and Weinberg[2] and Salam[3] in 1967, who in turn incorporated the Higgs mechanism in Glashow's electroweak interaction, giving an $SU(3) \times SU(2) \times U(1)$ gauge symmetry to the theory. Their results succeed in unifying three out of the four known forces, with no quantum theory for the gravitational force having been established yet.

The theory of the SM breaks the elementary particles into two main categories: the fermions, which interact with the force fields, and bosons, which are directly associated with the interaction fields, known as the force carriers. The fermions are known for having half-integer spin, whereas the bosons have integer spin. There exist five known bosons, the photon, associated with the EM interaction, the Z^0 and $W^{\pm}$ bosons for the weak interaction and the gluon for the strong interaction. The Higgs particle is also a boson, with spin zero and it represents the immediate field that gives mass to the rest elementary particles. The fermions, on the other hand, are bigger in number and are defined as leptons and quarks. They are grouped into three generations, with each generation consisting of two quarks and two leptons, which share similar properties. Each generation's difference from its precedent is the larger mass of the fermions that it consists of. Lastly, each fermion has a corresponding anti-fermion, which has opposite charge.

Interacting field	Boson	Range	Relative strength
Electromagnetic	Photon (γ)	∞	$\frac{1}{137}$
Weak	$W^{\pm}, Z^0$	10^{-3} fm	10^{-6}
Strong	Gluon (g)	1fm	1
Gravitational	Graviton[1]	∞	10^{-43}

Table 1: Carriers and basic properties of the four fundamental interactions.

1.2 Quantum Chromodynamics

Out of the four interactive fields, the strong interaction is, as the name suggests, the strongest. The Quantum Field Theory (QFT) describing it is known as Quantum Chromodynamics (QCD). Its purpose is to give the theoretical background behind the interactions involving quarks and gluons and its name stems from the fact that strong interactions are sensitive to color, a type of charge that both quarks and gluons carry. QCD is a gauge theory, based on the unbroken non-abelian $SU(3)$ group [4]. Since an $SU(3)$ group has eight generators, there can exist eight gluons, carrying color charge, which mediate the strong force among the quarks. No quark has ever been observed free in nature, but all are confined within hadrons, which have a net neutral color. This

[1]Hypothetical particle. Not observed yet.

property of QCD can be explained by the asymptotic freedom that describes it, which tells us that the forces acting between quarks in small separations become weak [5],[6],[7]. In addition, quark confinement can also be explained by the property of the non-abelian gluons to couple to themselves. Given the asymptotic freedom that describes our theory, the coupling strength could become large in large quark separations, which could explain why these fundamental particles can not be described by a free field theory.

The study of QCD was, until 1974 done perturbatively. Non-perturbative numerical methods were introduced by K. Wilson, proposing a lattice formulation to explain and further research the quark confinement and asymptotic freedom of the strong interaction [8]. With this approach, which has become widely used in QCD works, one can introduce numerical simulations to calculate quantum mechanical properties of a strongly interacting system, using the path integral formalism.

1.3 Path integral approach

1.3.1 The Feynman Path integral for a continuum theory

The path integral, a concept introduced by R. Feynman, has proven to be a very powerful tool when studying quantum mechanical systems, as it allows us to calculate the spectrum of Euclidean operators acting in a Hilbert space. We begin the introduction of the path integral by defining the Euclidean correlator of two operators, $\widehat{O}_1, \widehat{O}_2$ as

$$\langle O_2(t)O_1(t)\rangle_T = \frac{1}{Z_T}\mathrm{tr}[e^{-(T-t)\widehat{H}}\widehat{O}_2 e^{-t\widehat{H}}\widehat{O}_1]\,, \tag{1.1}$$

where $\widehat{H}$ is the Hamiltonian of the system, generally given by $\hat{H} = \frac{\hat{p}^2}{2m} + \hat{U}$ and Z_T is the partition function, defined as

$$Z_T = \mathrm{tr}[e^{-T\widehat{H}}]\,. \tag{1.2}$$

What we aim for, using Equation 1.1, is to derive an equation that will, eventually, enable us to extract the matrix elements and energy spectrum of the operators and states of the theory we are studying. Referring to Equation A.7 from Appendix A, and the eigenvalue equation ($\widehat{H}|e_n\rangle = E_n|e_n\rangle$) one can show that

$$Z_T = \sum_n \langle e_n|e^{-T\widehat{H}}|e_n\rangle = \sum_n e^{-TE_n}\,. \tag{1.3}$$

The same procedure can be used for the numerator on the Euclidean correlator function, by inserting the unit operator as defined in Equation A.4, between $\widehat{O}_2$ and $\widehat{O}_1$. Expanding the numerator and denominator in terms of the exponential containing the ground state, we get

$$\begin{aligned} \langle O_2(t)O_1(t)\rangle_T &= \frac{1}{Z_T}\sum_{n,m} e^{-(T-t)E_m}e^{-tE_n}\langle e_m|\widehat{O_2}|e_n\rangle\langle e_n|\widehat{O_1}|e_m\rangle \\ \Rightarrow \langle O_2(t)O_1(t)\rangle_T &= \frac{\sum_{n,m} e^{-(T-t)\Delta E_m}e^{-t\Delta E_n}\langle e_m|\widehat{O_2}|e_n\rangle\langle e_n|\widehat{O_1}|e_m\rangle}{1 + e^{-T\Delta E_1} + e^{-T\Delta E_2} + ...}\,. \end{aligned} \tag{1.4}$$

Finally, taking the limit of the above equation for large T, the denominator simplifies to 1 and we are left with

$$\lim_{T\to\infty}\langle O_2(t)O_1(t)\rangle_T = \sum_n \langle 0|\widehat{O}_2|e_n\rangle\langle e_n|\widehat{O}_1|0\rangle e^{-tE_n}\,, \tag{1.5}$$

where cases with $m \neq 0$ no longer contribute to the correlator and the vacuum state, E_0, has now been normalized to 0.
We now move on to introducing an expression for the above equation using the path integral. We define the partition function for a one-dimensional system as the integral

$$Z_T = \int dx \langle x|e^{-T\hat{H}}|x\rangle \,. \tag{1.6}$$

Introducing momentum states, $|p\rangle$, between the position states, $|x\rangle$, will enable us to use plane wave representation in the integral:

$$\langle x|e^{-T\hat{H}}|y\rangle = \int dp \, \langle x|e^{-T\hat{H}}|p\rangle\langle p|y\rangle \,. \tag{1.7}$$

The problem here is that for a system in nonzero potential, the matrix element $\langle x|e^{-T\hat{H}}|p\rangle$ is poorly defined, since $\hat{U}$ and $\hat{p}$ don't necessarily commute. To account for this, we split the potential symmetrically, and expand the exponential for an infinitesimal timestep ε

$$e^{-\varepsilon\hat{H}} = e^{-\varepsilon\hat{U}/2}e^{-\varepsilon\hat{p}^2/2m}e^{-\varepsilon\hat{U}/2}(1+\mathcal{O}(\varepsilon)) \,. \tag{1.8}$$

We define $\widehat{W}_\varepsilon$ as the leading term of the expansion, namely $\widehat{W}_\varepsilon = e^{-\varepsilon\hat{U}/2}e^{-\varepsilon\hat{p}^2/2m}e^{-\varepsilon\hat{U}/2}$.
We then rewrite the matrix element of Equation 1.7 , using $\widehat{W}_\varepsilon$:

$$\begin{aligned}
\langle x|\widehat{W}_\varepsilon|y\rangle &= \int dp \, \langle x|e^{-\varepsilon\hat{U}/2}e^{-\varepsilon\hat{p}^2/2m}e^{-\varepsilon\hat{U}/2}|p\rangle\langle p|y\rangle \\
&= e^{-\varepsilon U(x)/2} \, e^{-\varepsilon U(y)/2} \int dp \, \langle x|p\rangle\langle p|y\rangle e^{-\varepsilon p^2/2m} \\
&= \sqrt{\frac{m}{2\pi\varepsilon}} \, e^{-\varepsilon U(x)/2} \, e^{-\varepsilon U(y)/2} e^{-(x-y)^2 m/2\varepsilon} \,,
\end{aligned} \tag{1.9}$$

where we have used that $\langle x|y\rangle = \frac{1}{\sqrt{2\pi}}e^{ipx}$ to evaluate the integral.
Also using that

$$e^{-T\hat{H}} = \lim_{N_T\to\infty} \widehat{W}_\varepsilon^{N_T} \,, \text{with } \varepsilon = \frac{T}{N_T} \,, \tag{1.10}$$

we find an expression for the partition function such that

$$\begin{aligned}
Z_T &= \lim_{N_T\to\infty} \int dx \langle x|e^{\widehat{W}_\varepsilon^{N_T}}|x\rangle \\
&= \lim_{N_T\to\infty} C^{N_T} \int dx \, dx_1 \, \ldots \, dx_{N_T-1} \, \exp\left(-\varepsilon \sum_{j=0}^{N_T-1} \left(\frac{m}{2}\frac{(x_j - x_{j+1})^2}{\varepsilon^2} + U(x_j)\right)\right) \,,
\end{aligned} \tag{1.11}$$

where $C = \sqrt{\frac{m}{2\pi\varepsilon}}$
Finally, using periodicity, i.e., $x_{N_T} = x_0 = x$, the partition function is approximately

$$Z_T^\varepsilon = C^{N_T} \int dx \, dx_1 \ldots dx_{N_T-1} \exp\left(-\varepsilon \sum_{j=0}^{N_T-1} \left(\frac{m}{2}\left(\frac{x_{j+1}-x_j}{\varepsilon}\right)^2 + U(x_j)\right)\right) \,. \tag{1.12}$$

If the sum on the exponent is taken over continuous paths, it can be evaluated as an integral over $t = j\varepsilon$

$$\varepsilon \sum_{j=0}^{N_T-1} \left(\frac{m}{2} \left(\frac{x_{j+1} - x_j}{\varepsilon} \right)^2 + U(x_j) \right) = \int_0^T dt \, \left(\frac{m}{2} \dot{x}(t)^2 + U(x(t)) \right) + \mathcal{O}(\varepsilon) \,, \tag{1.13}$$

where we have defined

$$\left(\frac{x_{j+1} - x_j}{\varepsilon} \right) = \dot{x}(t) + \mathcal{O}(\varepsilon) \,. \tag{1.14}$$

From Equation 1.13 we get the mathematical formula for the action of the theory, called Euclidean action. It is derived from the regular action only by making a rotation from real to imaginary time, namely $t = i\tau$.

$$S[x, \dot{x}] = \int_0^T d\tau \, \left(\frac{m}{2} \dot{x}^2(\tau) - U(x(\tau)) \right) \xrightarrow{\tau \to -it} i \int_0^T dt \, \left(\frac{m}{2} \dot{x}^2(t) + U(x(t)) \right) = i S_E[x, \dot{x}] \,. \tag{1.15}$$

The different values x_j can be taken as different paths and the integral is calculated over all possible paths.

1.3.2 Path integral on the lattice

Our next goal is to apply what we have obtained from the regular path integral theory to a discretized space that describes a field theory. Since we are evaluating fields, the common operators of the Hamiltonian, $\hat{x}$ and $\hat{p}$, now become $\hat{\Phi}(x)$ and $\hat{\Pi}(x)$ respectively. By introducing a lattice space, Λ_3, the vector $\boldsymbol{x}$ becomes :

$$\boldsymbol{x} \to \alpha \boldsymbol{n}, \text{ where } n_i = 0, 1, \ldots, N-1, \text{ for } i = 1, 2, 3 \,. \tag{1.16}$$

The vectors n_i label the lattice points and α is the lattice constant, i.e., the space between two lattice points. Now, $\hat{\Phi}$ and $\hat{\Pi}$ *"live"* only on those lattice points. Their eigenstates are defined as

$$\begin{aligned} \widehat{\Phi}(\boldsymbol{n})|\Phi\rangle &= \Phi(\boldsymbol{n})|\Phi\rangle \,, \\ \widehat{\Pi}(\boldsymbol{n})|\Pi\rangle &= \Pi(\boldsymbol{n})|\Pi\rangle \,. \end{aligned} \tag{1.17}$$

The states are orthogonal and complete, in the sense that

$$\begin{aligned} &\langle \Phi|\Phi'\rangle = \delta(\Phi - \Phi') = \prod_{\boldsymbol{n}\in\Lambda_3} \delta(\Phi(\boldsymbol{n}) - \Phi'(\boldsymbol{n})) \,, \mathbb{1} = \int_\infty^\infty \mathcal{D}\Phi |\Phi\rangle\langle\Phi| \,, \text{where } \mathcal{D}\Phi = \prod_{\boldsymbol{n}\in\boldsymbol{\Lambda_3}} d\Phi(\boldsymbol{n}) \text{and} \\ &\langle \Pi|\Pi'\rangle = \delta(\Pi - \Pi') = \prod_{\boldsymbol{n}\in\Lambda_3} \delta(\Pi(\boldsymbol{n}) - \Pi'(\boldsymbol{n})) \,, \mathbb{1} = \int_\infty^\infty \mathcal{D}\Pi |\Pi\rangle\langle\Pi| \,, \text{where } \mathcal{D}\Pi = \prod_{\boldsymbol{n}\in\boldsymbol{\Lambda_3}} d\Pi(\boldsymbol{n}) \,. \end{aligned} \tag{1.18}$$

and the plane waves are now represented as

$$\langle \Phi|\Pi\rangle = \prod_{\boldsymbol{n}\in\Lambda_3} \sqrt{\frac{\alpha^3}{2\pi}} e^{i\alpha^3 \Pi(\boldsymbol{n})\Phi(\boldsymbol{n})} \,. \tag{1.19}$$

Lastly, the matrix element becomes

$$\langle\Phi|e^{-t\hat{H}}|\Phi'\rangle = \int \mathcal{D}\Pi\langle\Phi|e^{-t\hat{H}}|\Pi\rangle\langle\Pi|\Phi'\rangle\,. \tag{1.20}$$

Using the same approach as with the non-discretized interpretation, we can define the partition function as

$$Z_T = \int \mathcal{D}\Phi\langle\Phi|e^{-T\hat{H}}|\Phi\rangle = \lim_{N_T\to\infty}\int \mathcal{D}\Phi\langle\Phi|\widehat{W}_\varepsilon^{N_T}|\Phi\rangle\,, \tag{1.21}$$

where $\widehat{W}_\varepsilon^{N_T}$ is introduced in Equation 1.8. Again, introducing $N_T - 1$ sets of complete states between in our equation, we get

$$Z_T = C^{N^3N_T}\int \mathcal{D}\Phi\cdots\mathcal{D}\Phi_{N_T-1}e^{-S_E[\Phi]}\,. \tag{1.22}$$

If we choose to introduce a 4D lattice Λ defined as

$$\Lambda = \{(\boldsymbol{n}, n_4)|\boldsymbol{n}\in\Lambda_3, n_4 = 0, 1, \cdots, N_T - 1\}\,, \tag{1.23}$$

the partition function now becomes

$$Z_T = C^{N^3N_T}\int \mathcal{D}[\Phi]e^{-S_E[\Phi]},\ \text{where}\,\mathcal{D}[\Phi] = \prod_{(\boldsymbol{n},n_4)\in\Lambda}\mathrm{d}\Phi(\boldsymbol{n}, n_4)\,. \tag{1.24}$$

In respect to this, the correlator also changes as

$$\begin{aligned}\langle O_2(t)O_1(t)\rangle_T &= \frac{1}{Z_T}\mathrm{tr}[\widehat{W}_\varepsilon^{N_T-n_t}\widehat{O}_2\widehat{W}_\varepsilon^{n_t}\widehat{O}_1]\\ &= \frac{C^{N^3N_T}}{Z_T}\int \mathcal{D}[\Phi]e^{-S_E[\Phi]}O_2[\Phi(.,n_t)]O_1[\Phi(.,0)]\,.\end{aligned} \tag{1.25}$$

Since the constant term simplifies, it is easier to redefine the correlator and partition function as

$$\begin{aligned}\langle O_2(t)O_1(t)\rangle_T &= \frac{1}{Z_T}\int \mathcal{D}[\Phi]e^{-S_E[\Phi]}O_2[\Phi(.,n_t)]O_1[\Phi(.,0)]\\ Z_T &= \int \mathcal{D}[\Phi]e^{-S_E[\Phi]}\,.\end{aligned} \tag{1.26}$$

2 Lattice Quantum Chromodynamics

Quantum Chromodynamics becomes relatively challenging for calculations to be performed at low energies, due to the breaking of asymptotic freedom. Thus, perturbation theories can only be applied at high energies. The main solution is to use lattice techniques to discretize the theory, which allows us to calculate observables at low energies too, using appropriate simulations. This chapter gives a brief introduction to the steps used to properly form the lattice formulation of QCD.

2.1 The continuum action

In order to investigate how the fields of quarks and gluons interact, we have to calculate the QCD action involving them. The gluons are introduced as gauge fields

$$A_\mu(x)_{cd}\,, \tag{2.1}$$

whereas the quarks are described by Dirac 4-spinors

$$\psi^f(x)_{\substack{\alpha\\c}}\,,\ \bar{\psi}^f(x)_{\substack{\alpha\\c}}\,. \tag{2.2}$$

The gluon fields have a Lorentz index, μ and two color indices, c and d. They are represented by traceless, hermitian, 3×3 matrices. The quark fields have a Dirac index, given by α, a color index, c, and lastly a flavor index, $f = 1, 2, \ldots, 6$. In this representation, roman letters are assigned values 1,2,3 and Greek letters take values 1,2,3,4. In the Minkowskian approach, the two fields ψ and $\bar{\psi}$ are related by $\bar{\psi} = \psi^\dagger\gamma_0$, where γ_0 is the γ matrix related to time, however, in the Euclidean path integral, one has to integrate over two independent variables, ψ and $\bar{\psi}$. Both in the gluon and quark fields, the space-time position is denoted by x.
We can define the action as a sum of two independent actions, the gluonic and fermionic actions

$$S_{QCD} = S_G + S_F\,. \tag{2.3}$$

Both parts have to be gauge invariant under rotation of the color indices among the quarks and the gluons. As Yang, Mills suggested, [9], we can define an independent 3×3 complex matrix $\Omega(x)$ at each point x, which ought to be unitary and have $\det[\Omega(x)] = 1$. These are the requirements that define the special unitary group, SU(3) for 3×3 matrices, closed under matrix multiplication. It is characterized as non-abelian, since matrix multiplication is non-commutative. The theories using such groups are usually referred to as Yang-Mills theories. The basic properties SU(N) groups are given in B.3.2.

The gluon gauge action is defined as

$$S_G[A] = \frac{1}{2g^2}\int d^4x\,\mathrm{tr}[F_{\mu\nu}(x)F_{\mu\nu}(x)]\,, \tag{2.4}$$

where $F_{\mu\nu}$ is the field strength tensor given by the anti-commutator between covariant derivatives D_μ, D_ν:

$$F_{\mu\nu} = -\mathrm{i}[D_\mu(x), D_\nu(x)] \quad \text{and} \quad D_\mu(x) = \partial_\mu + \mathrm{i}A_\mu(x)\,. \tag{2.5}$$

As for the fermionic part, it is given by

$$S_F[\psi,\bar{\psi},A] = \sum_{f=1}^{N_f}\int d^4x\,\bar{\psi}^{(f)}(x)\left(\gamma_\mu(\partial_\mu + \mathrm{i}A_\mu(x)) + m^{(f)}\right)\psi^{(f)}(x)\,, \tag{2.6}$$

where we sum over all the different flavors.
We demand that the action is invariant under transformations of the gauge and fermion fields. We must therefore require invariance under the transformation

$$\psi(x) \to \psi'(x) = \Omega(x)\psi(x)\,,\ \bar{\psi}(x) \to \bar{\psi}(x)\Omega(x)^\dagger\,. \tag{2.7}$$

For the fermionic part, this reads

$$S_F[\psi, \bar{\psi}, A] = S_F[\psi', \bar{\psi}', A']\,, \tag{2.8}$$

which gives us the transformations the gluon field and the covariant derivative must undergo

$$\begin{aligned} A_\mu(x) &\to A'_\mu(x) = \Omega(x)A_\mu(x)\Omega(x)^\dagger + \mathrm{i}(\partial_\mu\Omega(x))\Omega^\dagger \\ D_\mu(x) &\to D'_\mu(x) = \Omega(x)D_\mu(x)\Omega(x)^\dagger\,. \end{aligned} \tag{2.9}$$

2.2 The discretized action

Following what was introduced in Chapter 1.3.2, we introduce the fermion fields on a 4D lattice Λ:

$$\Lambda = \{n = (n_1, n_2, n_3, n_4)\,|\,n_1, n_2, n_3 = 0, 1, \cdots, N-1; n_4 = 0, 1, \cdots, N_T - 1\}\,. \tag{2.10}$$

Each lattice point in space-time is separated by a lattice constant a, and is connected to the physical point x by $x = an$. The spinors and gauge fields are written as

$$\psi(n),\ \overline{\psi}(n),\ A_\mu(n), \quad n \in \Lambda\,. \tag{2.11}$$

2.2.1 Grassmann numbers and Fermi statistics

It is widely known that fermions obey Fermi anti-commutating statistics, i.e., the product of two fermions acquires a minus sign for a permutation between their quantum numbers. This relation must hold between combinations of ψ and $\bar{\psi}$:

$$\begin{aligned} \psi^{(f)}(n)_{a,\alpha}\psi^{(f')}(n')_{a',\alpha'} &= -\psi^{(f')}(n')_{a',\alpha'}\psi^{(f)}(n)_{a,\alpha}\,, \\ \overline{\psi}^{(f)}(n)_{a,\alpha}\overline{\psi}^{(f')}(n')_{a',\alpha'} &= -\overline{\psi}^{(f')}(n')_{a',\alpha'}\overline{\psi}^{(f)}(n)_{a,\alpha}\,, \\ \psi^{(f)}(n)_{a,\alpha}\overline{\psi}^{(f')}(n')_{a',\alpha'} &= -\overline{\psi}^{(f')}(n')_{a',\alpha'}\psi^{(f)}(n)_{a,\alpha}\,. \end{aligned} \tag{2.12}$$

Thus, it is helpful to introduce *Grassmann numbers* to describe the fermionic part of the action. We discuss the various properties of this set of numbers in this section.

A set of Grassmann numbers, $\eta_i, i = 1, \cdots, N$ obey the anti-commutating algebra

$$\eta_i\eta_j = -\,\eta_j\eta_i \quad \text{and} \quad \eta_i\eta_i = 0\,. \tag{2.13}$$

Functions consisting of polynomials of Grassmann numbers form a Grassmann algebra. In that case, η_i are known as the generators of the algebra.

$$A = a + \sum_i a_i\eta_i + \sum_{i<j} a_{ij}\eta_i\eta_j + \cdots + a_{12\cdots N}\eta_1\eta_2\cdots\eta_N\,. \tag{2.14}$$

Equation 2.14 gives an example of such a polynomial function, with the appropriate coefficients $a, a_i, \cdots, a_{12\cdots N} \in \mathbb{C}$.

It can be shown that the integral over such polynomial A is proportional to the coefficient of the highest order of the generators. The rest terms will vanish, since they can be written as derivatives of some other Grassmann polynomials, A' and such integrations yield zero. We demand that the integral is normalized, such that

$$\begin{gathered}\int d^N\eta\, \eta_1\eta_2\cdots\eta_N = 1, \quad \text{and} \quad \int d^N\eta\, A = a_{12\cdots N} \\ \text{with} \quad d^N\eta = d\eta_N\, d\eta_{N-1}\, \cdots d\eta_1\,.\end{gathered} \tag{2.15}$$

Under a linear transformation, Grassmann numbers become

$$\eta_i' = \sum_{j=1}^{N} M_{ij}\eta_j, \quad \text{with } M \text{ an } N\times N \text{ complex matrix}\,. \tag{2.16}$$

One can show that the measure of the Grassmann integration, $d^N\eta$ transforms as

$$d^N\eta' = \det[M]\, d^N\eta'\,. \tag{2.17}$$

The expectation value of a function of products of Grassmann numbers, such as the fermionic expectation value, also known as an n-point function, can be computed using Wick's theorem:

$$\begin{aligned}\langle \eta_{i_1}\overline{\eta}_{j_1}\cdots\eta_{i_n}\overline{\eta}_{j_n}\rangle_F &= \frac{1}{Z_F}\int \prod_{k=1}^{N} d\eta_k\, d\bar{\eta}_k\, \eta_i\overline{\eta}_j\cdots\eta_{i_n}\overline{\eta}_{j_n}\exp\left(\sum_{l,m=1}^{N}\bar{\eta}_l M_{lm}\eta_m\right) \\ &= (-1)^n \sum_{P(1,2,\cdots,n)} \text{sign}(P)\left(M^{-1}\right)_{i_1 j_{P_1}}\left(M^{-1}\right)_{i_2 j_{P_2}}\cdots\left(M^{-1}\right)_{i_n j_{P_n}}\,,\end{aligned} \tag{2.18}$$

where the sum is taken over all permutations $P(1,2,\cdots,n)$. It is beneficial to also utilize a different approach and rewrite the partition function,Z_F, using the Matthews-Salam formula[10, 11]

$$Z_F = \int d\eta_N\, d\bar{\eta}_N\, \cdots\, d\eta_1\, d\bar{\eta}_1\, \exp\left(\sum_{i,j=1}^{N}\bar{\eta}_i\, M_{ij}\,\eta_j\right) \,=\, \det[M]\,. \tag{2.19}$$

One can also replace the integral with partial derivatives with respect to the source terms of the generating functional for fermions, $W[\theta,\bar{\theta}]$:

$$\begin{gathered}\langle \eta_{i_1}\overline{\eta}_{j_1}\cdots\eta_{i_n}\overline{\eta}_{j_n}\rangle_F = \frac{1}{Z_F}\frac{\partial}{\partial\theta_{j_1}}\frac{\partial}{\partial\bar{\theta}_{i_1}}\cdots\frac{\partial}{\partial\theta_{j_n}}\frac{\partial}{\partial\bar{\theta}_{i_n}}\,W[\theta,\bar{\theta}]\Big|_{\theta,\bar{\theta}=0}\quad, \text{where} \\ W[\theta,\bar{\theta}] = \det[M]\exp\left(-\sum_{n,m=1}^{N}\bar{\theta}_n\,(M^{-1})_{nm}\,\theta_m\right)\,.\end{gathered} \tag{2.20}$$

2.2.2 Naive discretization of free fermions

The transition from continuum to lattice space does not only change the definition of the fermion and gauge fields, but that of the partial derivative as well. In the discretized case it transforms as

$$\partial_\mu\psi(x) \to \frac{1}{2a}\left(\psi(n+\hat{\mu}) - \psi(n-\hat{\mu})\right)\,. \tag{2.21}$$

Thus, the action for free fermions on the lattice becomes

$$S_F^0[\psi,\bar{\psi}] = a^4 \sum_{n\in\Lambda} \bar{\psi}(n) \left(\sum_{\mu=1}^{4} \gamma_\mu \frac{\psi(n+\hat{\mu}) - \psi(n-\hat{\mu})}{2\alpha} + m\,\psi(n) \right) . \tag{2.22}$$

Applying the field transformation we have introduced in Equation 2.7 to the discretized case, the partial derivative term of the action is not gauge invariant. Instead, it shall become

$$\bar{\psi}(n)\psi(n\pm\hat{\mu}) \to \bar{\psi}'(n)\psi'(n\pm\hat{\mu}) = \bar{\psi}(n)\Omega(n)^\dagger\Omega(n\pm\hat{\mu})\psi(n\pm\hat{\mu})\,. \tag{2.23}$$

2.2.3 Introducing link variables on the lattice

In order to resolve this issue, we introduce *link variables*, $U_\mu(n)$, which are $SU(3)$ gauge group elements, attached on the lattice links, and which can transform as shown below:

$$U_\mu(n) \to U'_\mu(n) = \Omega(n)U_\mu(n)\Omega(n+\hat{\mu})^\dagger\,. \tag{2.24}$$

They connect the lattice sites n with $n+\hat{\mu}$. One can also define the link variable pointing to the opposite direction:

$$\begin{aligned} &U_{-\mu}(n) = U_\mu(n-\hat{\mu})^\dagger \text{ ,which transforms as} \\ &U_{-\mu}(n) \to U'_{-\mu}(n) = \Omega(n)U_{-\mu}\Omega(n-\hat{\mu})^\dagger\,. \end{aligned} \tag{2.25}$$

Thus, the transformation

$$\bar{\psi}'(n)U'_\mu(n)\psi'(n) \to \bar{\psi}(n)U_\mu(n)\psi(n) \tag{2.26}$$

ensures gauge invariance.

The link variables can also be interpreted as the lattice version of a gauge transporter, connecting two points, x and y, or n and $n+\hat{\mu}$ for the discretized case. A gauge transporter can be expressed as

$$G(x,y) = \exp\left(\mathrm{i}\int A\cdot \mathrm{ds}\right) \to U_\mu(n) = \exp\left(\mathrm{i}\alpha A_\mu(n)\right)\,, \tag{2.27}$$

where in the lattice version, we have substituted the integral with the approximation $aA_\mu(n)$. Given that we are working towards a generalization of our results to the limit where $a \to 0$, we can expand the exponential in terms of α

$$U_\mu(n) = \mathbb{1} + \mathrm{i}\alpha A_\mu(n) + \mathcal{O}(\alpha^2),\ U_{-\mu}(n) = \mathbb{1} - \mathrm{i}\alpha A_\mu(n-\hat{\mu}) + \mathcal{O}(\alpha^2)\,. \tag{2.28}$$

In addition, we can also approximate the behavior of the fermion and gauge fields as

$$\psi(n\pm\hat{\mu}) = \psi(n) + \mathcal{O}(\alpha) \quad \text{and} \quad A_\mu(n-\hat{\mu}) = A_\mu(n) + \mathcal{O}(\alpha)\,. \tag{2.29}$$

Applying these to the fermionic action, we end up with two terms which add up to $S_F[\psi,\bar{\psi},U]$: the free part, $S_F^0[\psi,\bar{\psi}]$, and the interaction part, $S_F^I[\psi,\bar{\psi},A]$.

$$\begin{aligned} &S_F[\psi,\bar{\psi},U] = S_F^0[\psi,\bar{\psi}] + S_F^I[\psi,\bar{\psi},A], \text{where} \\ &S_F^0[\psi,\bar{\psi}] = \alpha^4 \sum_{n\in\Lambda} \bar{\psi}(n) \left(\sum_{\mu=1}^{4} \gamma_\mu \frac{U_\mu(n)\psi(n+\hat{\mu}) - U_{-\mu}(n)\psi(n-\hat{\mu})}{2\alpha} + m\psi(n) \right) , \\ &S_F^I[\psi,\bar{\psi},A] = \mathrm{i}\alpha^4 \sum_{n\in\Lambda}\sum_{\mu=1}^{4} \bar{\psi}(n)\gamma_\mu A_\mu(n)\psi(n) + \mathcal{O}(\alpha)\,. \end{aligned} \tag{2.30}$$

2.3 The Wilson gauge action

We have shown how the introduction of link variables is the starting point for adding gluon fields on the lattice. We now move on to assemble the lattice gauge action, making use of the link variables and showing that at the continuum limit, it returns the correct format. We stress that this does not represent the full quantum theory, rather it is merely the naive continuum limit.

2.3.1 Creating Gauge-invariant objects with link variables

The product of link variables alongside a path of links $\mathcal{P}$, connecting the points n_0 and n_1 is the lattice equivalent of the continuum gauge transporter. The string of such link variables is given by the product

$$P[U] \equiv \prod_{(n,\mu)\in\mathcal{P}} U_\mu(n)\,. \tag{2.31}$$

Following the transformation properties of link variables, under a gauge transformation it becomes

$$P[U] \rightarrow\ P[U'] = \Omega(n_0)P[U]\Omega(n_1)^\dagger\,. \tag{2.32}$$

It is evident that attaching two appropriate fermion fields on each side of P[U], the product becomes gauge invariant:

$$\bar{\psi}(n_0)P[U]\psi(n_1) = \bar{\psi}'(n_0)P[U']\psi'(n_1)\,. \tag{2.33}$$

One can also construct a gauge invariant product of link variables, defining the path $\mathcal{P}$ on a closed loop $\mathcal{L}$ and taking the trace of the product

$$L[U] = \mathrm{tr}\left[\prod_{(n,\mu)\,\in\,\mathcal{L}} U_\mu(n)\right]\,. \tag{2.34}$$

Under a gauge transformation, like in Equation 2.32, the product will remain unaffected, due to the commutative properties of the trace:

$$\begin{aligned} L[U'] &= \mathrm{tr}\left[\Omega(n_0)\prod_{(n,\mu)\in\mathcal{L}} U_\mu(n)\Omega(n_0)^\dagger\right] \\ &= \mathrm{tr}\left[\Omega(n_0)\Omega(n_0)^\dagger\prod_{(n,\mu)\in\mathcal{L}} U_\mu(n)\right] \\ &= \mathrm{tr}\left[\prod_{(n,\mu)\in\mathcal{L}} U_\mu(n)\right] \\ &= L[U]\,. \end{aligned} \tag{2.35}$$

These loops are used to derive a format for the gluon action.

2.3.2 The Gauge action

For a single flavor, we have shown that the fermionic action is gauge invariant if we introduce link variables to it. For the gluonic part, we must look for objects utilizing the link variables, that would return the continuum action when taking $a \to 0$. We opt to use the plaquette variable $U_{\mu\nu}$, which is a product of four link variables, creating a closed loop along the lattice links:

$$\begin{aligned} U_{\mu\nu}(n) &= U_\mu(n)U_\nu(n+\hat{\mu})U_{-\mu}(n+\hat{\mu}+\hat{\nu})U_{-\nu}(n+\hat{\nu}) \\ &= U_\mu(n)U_\nu(n+\hat{\mu})U_\mu(n+\hat{\nu})^\dagger U_\nu(n)^\dagger \,. \end{aligned} \tag{2.36}$$

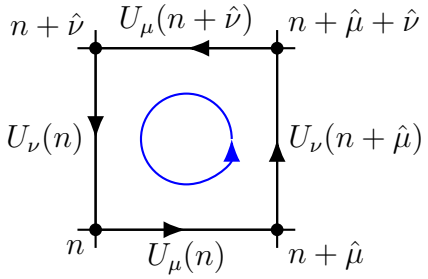

Figure 1: The four link variables used to create the plaquette $U_{\mu\nu}(n)$. The blue circle shows the order of the appearance of the link variables in the plaquette.

One can show that the trace of the plaquette over the closed loop is gauge invariant. Now, the Wilson gauge action is a sum over all plaquettes, with each counted in one orientation. The general expression for the Wilson action can be generalized by a sum over all points n as well as a sum over the four Lorentz indices

$$S_G[U] = \frac{2}{g^2} \sum_{n\in\Lambda} \sum_{\mu<\nu} \mathrm{Re}\ \mathrm{tr}[\mathbb{1} - U_{\mu\nu}(n)] \,. \tag{2.37}$$

The plaquettes, being formed by link variables, are exponentials of the gauge field $A_\mu(n)$. Expanding them using the Baker-Campbell-Haussdorf formula, and performing a Taylor expansion on the gauge fields, we derive

$$\begin{aligned} U_{\mu\nu} &= \exp(\mathrm{i}a^2(\partial_\mu A_\nu(n) - \partial_\nu A_\mu(n) + \mathrm{i}[A_\mu(n), A_\nu(n)] + \mathcal{O}(a^3) \\ U_{\mu\nu} &= \exp(\mathrm{i}a^2 F_{\mu\nu} + \mathcal{O}(a^3)) \,. \end{aligned} \tag{2.38}$$

For small α^2, we can expand the exponential as well. Equation 2.37 now becomes

$$S_G[U] = \frac{\alpha^4}{2g^2} \sum_{n\in\Lambda} \sum_{\mu,\nu} \mathrm{tr}[F_{\mu\nu}(n)^2] + \mathcal{O}(\alpha^2) \,. \tag{2.39}$$

2.4 Improving the fermion action

Although the previous discussion gives appropriate results for the formulation of fermions on the lattice, it can not be the final result. There are still some lattice artifacts we need to evaluate and remove, known as *doublers*, in order to obtain the correct form.

2.4.1 The Dirac operator on the lattice

The free part of the fermion action of Equation 2.30 can be written in the form of

$$S_F[\psi,\bar{\psi},U] = \alpha^4 \sum_{n,m\in\Lambda}\sum_{a,b,\alpha,\beta} \bar{\psi}(n)_{a,\alpha} D(n|m)_{a,\alpha,b,\beta}\, \psi(n)_{b,\beta}\,, \tag{2.40}$$

where we introduce $D(n|m)$ as the naive Dirac operator on the lattice. It is described by

$$D(n|m)_{ab,\alpha\beta} = \sum_{\mu=1}^{4} (\gamma_\mu)_{\alpha,\beta} \frac{U_\mu(n)_{a,b}\delta_{n+\hat{\mu},m} - U_{-\mu}(n)_{ab}\delta_{n-\hat{\mu},m}}{2\alpha} + m\,\delta_{\alpha,\beta}\,\delta_{a,b}\,\delta_{n,m}\,. \tag{2.41}$$

Using this notation, we can work out immediately the relation between the action and Wick's theorem. In fact, setting $M = -a^4 D$, it is obvious that apart from the summation over the several Dirac and color indices, the format is the same.

2.4.2 The doubling problem

The problem with the Dirac operator we have constructed on the lattice arises when we compute the Fourier transform of its inverse, the quark propagator $D^{-1}(n|m)$. Although on the continuum case the quark propagator for free massless fermions ($U_{\mu\nu} = \mathbb{1}, m = 1$) returns a pole at $p = (0,0,0,0)$, for the lattice case, however, we obtain additional poles whenever a direction of p equals $\pm\pi/a$. This generates 15 unwanted poles, also known as doublers.
In general, the Fourier transform of the Dirac operator will be given by

$$\begin{aligned}
\widetilde{D}(p|q) &= \frac{1}{|\Lambda|}\sum_{n,m\in\Lambda} e^{-ip\cdot n\alpha} D(n|m) e^{iq\cdot\ m\alpha} \\
&= \frac{1}{|\Lambda|}\sum_{n,m\in\Lambda} e^{-i(p-q)\alpha}\left(\sum_{\mu=1}^{4}\gamma_\mu \frac{e^{iq_\mu\alpha}-e^{-iq_\mu\alpha}}{2\alpha} + m\mathbb{1}\right) \\
&= \delta(p-q)\widetilde{D}(p), \quad \text{where} \\
\widetilde{D}(p) &= +m\mathbb{1} + \sum_{\mu=1}^{4}\gamma_\mu \sin(p_\mu\alpha)\,,
\end{aligned} \tag{2.42}$$

with $|\Lambda|$ the total number of lattice points. The inverse of the Fourier transformed Dirac operator gives

$$\widetilde{D}(p)^{-1} = \frac{m\mathbb{1} - i\alpha^{-1}\sum_\mu \gamma_\mu \sin(p_\mu\,\alpha)}{m^2 + \alpha^{-2}\sum_\mu \sin^2(p_\mu\alpha)}\,. \tag{2.43}$$

It is easy to understand that the doublers appear due to the $\sin(p_\mu a)$ factors. One may also take the continuum limit $a \to 0$ to show that this problem is eliminated in the continuum case

$$\widetilde{D}(p)^{-1}\Big|_{m=0} \xrightarrow{a\to 0} \frac{-i\sum_\mu \gamma_\mu\, p_\mu}{p^2}\,. \tag{2.44}$$

2.4.3 Introducing Wilson fermions

The previous discussion leads us to the conclusion that we need to introduce an extra fermionic term that vanishes when $p_\mu = 0$, but is nonzero when $p_\mu = \pi/a$. Wilson

suggested that this term should transform the Dirac operator as

$$\widetilde{D}(p) = m\mathbb{1} + \frac{i}{\alpha}\sum_{\mu=1}^{4}\gamma_\mu \sin(p_\mu\alpha) + \mathbb{1}\frac{1}{\alpha}\sum_{\mu=1}^{4}(1-\cos(p_\mu\alpha))\,. \tag{2.45}$$

This extra term, often referred to as Wilson term, acts like an additional mass term when $p_\mu = \pi/a$, with the total mass of the doubler being $m+\frac{2l}{a}$ with l the number of momentum components with $p_\mu = \pi/a$. As a approaches zero, the doublers' mass becomes very large and they decouple from the theory. Calculating $\widetilde{D}(p)^{-1}$, we find that the only pole left is when $p = (0,0,0,0)$.
We can find the expression for the Wilson term in the Dirac operator by computing its inverse Fourier transform. Inserting link variables to the transformation to make the expression gauge invariant, one obtains

$$-\alpha\sum_{\mu=1}^{4}\frac{U_\mu(n)_{a,b}\delta_{n+\hat{\mu},m} - 2\delta_{a,b}\,\delta_{n,m} + U_{-\mu}(n)_{a,b}\delta_{n-\hat{\mu},m}}{2\alpha^2}\,. \tag{2.46}$$

We can add this term to the initial expression of the Dirac operator and finally, for a single flavor (f), get

$$D^{(f)}(n|m)_{ab,\alpha\beta} = \left(m^{(f)}+\frac{4}{\alpha}\right)\delta_{\alpha\beta}\delta_{ab}\delta_{mn} - \frac{1}{2\alpha}\sum_{\mu=\pm1}^{\pm4}(\mathbb{1}-\gamma_\mu)_{\alpha\beta}\,U_\mu(n)_{ab}\delta_{n+\hat{\mu},m}\,. \tag{2.47}$$

2.4.4 Hopping expansion of the quark propagator

In the limit of large quark masses, the Dirac operator can be written as

$$\begin{aligned} &D = C(\mathbb{1}-\kappa H), \quad \text{where} \quad C = m+\frac{4}{\alpha}, \quad \kappa = \frac{1}{2(\alpha m+4)} \quad \text{and} \\ &H = H(n|m)_{\alpha\beta,ab} = \sum_{\mu=\pm1}^{\pm4}(\mathbb{1}-\gamma_\mu)_{\alpha\beta}U_\mu(n)_{ab}\delta_{n+\hat{\mu}+m}\,. \end{aligned} \tag{2.48}$$

The term H collects the nearing neighbors in the Dirac operator, and thus it is called the hoping matrix, whereas κ is the hopping parameter. Choosing to absorb C on the definition of the quark fields, ψ, we obtain the Dirac operator and its inverse in the form

$$\begin{aligned} D &= (\mathbb{1}-\kappa H)\,, \\ D^{-1} &= (\mathbb{1}-\kappa H)^{-1}\,. \end{aligned} \tag{2.49}$$

For large mas, the hopping parameter becomes relatively small, and thus we can expand the inverse Dirac operator in power series of κ : $D^{-1} = \sum_{j=0}^{\infty}\kappa^j H^j$, which converges when $\kappa||H|| < 1$. With this evaluation we can interpret the hopping parameter κ as a path between the two points n and m. A the order in κ increases, the corresponding path contributions also become longer.

2.5 Discrete symmetries of the Wilson action

One limitation to the discretization of lattice is the breaking of many symmetries that hold in the continuum limit, such as translation or rotation invariance. However, discrete symmetries like those of charge conjugation and parity still hold.

2.5.1 Charge conjugation

When the charge conjugation operator acts on particle wavefunction, it transforms it into its antiparticle. On the Dirac spinor fields, we get:

$$\begin{aligned} \psi(n) &\xrightarrow{\mathcal{C}} \psi(n)^{\mathcal{C}} = C^{-1}\overline{\psi}(n)^T\,, \\ \overline{\psi}(n) &\xrightarrow{\mathcal{C}} \overline{\psi}(n)^{\mathcal{C}} = -\psi(n)^T C\,. \end{aligned} \tag{2.50}$$

On the link variables, the charge conjugation acts as

$$U_\mu(n) \xrightarrow{\mathcal{C}} U_\mu(n)^{\mathcal{C}} = U_\mu(n)^* = (U_\mu(n)^\dagger)^T\,. \tag{2.51}$$

Recalling that the link variable is an exponential of the gauge field (Eq. 2.27), the change can be evaluated as the transformation $A_\mu(n) \to -A_\mu(n)^T$, which corresponds to a particle with opposite charge, concluding that an antiparticle has the opposite charge of the particle.

The charge conjugation matrix is defined from the relation

$$C\gamma_\mu C^{-1} = -\gamma_\mu^T\,. \tag{2.52}$$

Its chiral representation is

$$C = \mathrm{i}\gamma_2\gamma_4\,, \tag{2.53}$$

where γ_2,γ_4, are Gamma Matrices, the properties of which are given in Appendix C. The charge conjugation matrix is therefore a hermitian, unitary matrix. We can use these properties of this matrix representation to show that the Wilson action is indeed invariant under charge conjugation.

2.5.2 Parity

On the continuum limit, a parity transformation results in the mirror of the spatial coordinates of the initial state. On the lattice, it gives

$$\begin{aligned} \psi(\boldsymbol{n}, n_4) &\xrightarrow{\mathcal{P}} \psi(\boldsymbol{n}, n_4)^{\mathcal{P}} = \gamma_4\psi(-\boldsymbol{n}, n_4)\,, \\ \overline{\psi}(\boldsymbol{n}, n_4) &\xrightarrow{\mathcal{P}} \overline{\psi}(\boldsymbol{n}, n_4)^{\mathcal{P}} = \overline{\psi}(-\boldsymbol{n}, n_4)\gamma_4\,, \\ U_i(\boldsymbol{n}, n_4) &\xrightarrow{\mathcal{P}} U_i(\boldsymbol{n}, n_4)^{\mathcal{P}} = U_i(-\boldsymbol{n} - \hat{i}, n_4)^\dagger\,, \\ U_4(\boldsymbol{n}, n_4) &\xrightarrow{\mathcal{P}} U_4(\boldsymbol{n}, n_4)^{\mathcal{P}} = U_4(-\boldsymbol{n}, n_4)\,. \end{aligned} \tag{2.54}$$

The proof that the Wilson action is invariant under parity transformation is a bit more tricky, because one has to redefine the lattice space Λ, so lattice points pointing to the negative direction can exist. It is trivial that the diagonal term is invariant. For the hopping term,

Apart from the transformation acting on the three spatial components of the fields, we can show similarly that the action is invariant under the general transformations $\mathcal{P}_\mu$, $\mu = 1, 2, 3, 4$, which are given by

$$\begin{aligned} \psi(n) &\xrightarrow{\mathcal{P}_\mu} \psi(n)^{\mathcal{P}_\mu} = \gamma_\mu\psi(P_\mu(n)), \\ \overline{\psi}(n) &\xrightarrow{\mathcal{P}_\mu} \overline{\psi}(n)^{\mathcal{P}_\mu} = \overline{\psi}(P_\mu(n))\gamma_\mu, \\ U_\nu(n) &\xrightarrow{\mathcal{P}_\mu} U_\nu(n)^{\mathcal{P}} = U_\nu(P_\mu(n) - \hat{\nu})^\dagger, \quad \mu \neq \nu \\ U_\mu(n) &\xrightarrow{\mathcal{P}_\mu} U_\mu(n)^{\mathcal{P}_\mu} = U_\mu(P_\mu(n))\,. \end{aligned} \tag{2.55}$$

with $P_\mu(n)$ reversing the sign of all coordinates except for the μ^{th}.

2.5.3 γ_5 - hermiticity

Lastly, we take a look on hermiticity: Most Dirac operators are γ_5-hermitian, meaning

$$(\gamma_5 D)^\dagger = \gamma_5 D \quad \Leftrightarrow \quad D^\dagger = \gamma_5 D \gamma_5 \,. \tag{2.56}$$

The diagonal part of the Wilson action is real, so it is in fact not affected from this symmetry. The hoping parameter, once again demands a closer look. We can show that a γ-matrix will transform as

$$\gamma_5 \gamma_\mu \gamma_5 = -\gamma_\mu \,. \tag{2.57}$$

Thus, the hoping term will take the form

$$\begin{aligned} &\sum_{\mu\pm1}^{\pm4} (\mathbb{1} + \gamma_\mu)_{\alpha\beta} \, U_\mu(n)_{ab} \delta_{n+\hat{\mu},m} = \sum_{\mu\pm1}^{\pm4} (\mathbb{1} - \gamma_\mu)_{\alpha\beta} \, U_{-\mu}(n)_{ab} \delta_{n-\hat{\mu},m} \\ =&\sum_{\mu\pm1}^{\pm4} (\mathbb{1} - \gamma_\mu)_{\alpha\beta} \, U_\mu(n-\hat{\mu})^\dagger_{ab} \delta_{n-\hat{\mu},m} = \sum_{\mu\pm1}^{\pm4} (\mathbb{1} - \gamma_\mu)_{\alpha\beta} \, U_\mu(m)^\dagger_{ab} \delta_{n,m+\hat{\mu}} \,. \end{aligned} \tag{2.58}$$

which is identical to its form in Equation 2.47. This property, which holds both for the Dirac operator and the quark propagator and it turns out to become essential when calculating hadron correlation functions.

2.6 The path integral of QCD

Having obtained two equations for both actions of our theory, we can write the Euclidean correlators in the form of a lattice path integral:

$$\begin{aligned} \langle O_2(t)\, O_1(0) \rangle &= \frac{1}{Z} \int \mathcal{D}[\psi, \bar{\psi}] \mathcal{D}[U] \, \exp\left(-S_F[\psi, \bar{\psi}, U] - S_G[U]\right) O_2[\psi, \bar{\psi}, U] O_1[\psi, \bar{\psi}, U], \text{with} \\ Z &= \int \mathcal{D}[\psi, \bar{\psi}] \mathcal{D}[U] \, \exp\left(-S_F[\psi, \bar{\psi}, U] - S_G[U]\right) \,. \end{aligned} \tag{2.59}$$

The integrations are performed over products of the fermion-antifermion fields and link variables:

$$\mathcal{D}[\psi, \bar{\psi}] = \prod_{n \in \Lambda} d\psi(n) \, d\bar{\psi}(n), \quad \mathcal{D}[U] = \prod_{n \in \Lambda} \prod_{\mu=1}^{4} dU_\mu(n) \,. \tag{2.60}$$

3 Numerical simulations and Lattice techniques

The analysis of certain observables on the lattice can be done through several procedures using statistical methods applied on the computer. In order to evaluate correctly the results, one has to follow several steps to ensure the results reach a sufficient equilibrium state. In this section we focus on describing the basic ideas of numerical methods used in lattice QCD.

3.1 Numerical simulations

3.1.1 Monte Carlo importance sampling

The Euclidean path integrals we wish to calculate are high-dimensional integrals over the field variables. For example, on a 10^4 space-time lattice, one has to account fro 4×10^4 link variables. Since in our case we are interested in the SU(3) theory, where each link variable introduces 8 real parameters, this yields 320,000 integrations to be done, which is impossible for us to do. Instead, we introduce probability theory, to replace the integral over a function,$f(x)$ with the average of the function values $f(x_n)$ at randomly chosen x_n, according to a distribution with density $\rho(x_n)$. The expectation value of the function $f(x)$ is given by

$$\langle f \rangle_\rho = \frac{\int_a^b \rho(x) f(x) dx}{\int_a^b \rho(x) dx} = \lim_{N \to \infty} \frac{1}{N} \sum_{n=1}^{N} f(x_n) \,. \tag{3.1}$$

Using this method, we have replaced the exact mean by a sample mean. This is the general idea of the importance sampling Monte Carlo method, where we approximate the sum by a small subset of configurations, which are sampled according to a weight factor - the distribution density. The path integral is of the same form as the left-hand side of Equation 3.1, so, we can write the expectation value of an operator as

$$\langle \mathcal{O} \rangle = \lim_{N \to \infty} \frac{1}{N} \sum_{n=1}^{N} O[U_n] \,, \tag{3.2}$$

where each U_n is sampled according to the probability distribution density

$$dP(U) = \frac{e^{-S[U]} \mathcal{D}[U]}{\int \mathcal{D}[U] e^{-S[U]}} \,, \tag{3.3}$$

where the exponential factor $e^{-S[U]}$ is the weight factor containing the action of the theory, similar to the Boltzmann factor in statistical mechanics. It can be proven that for statistically independent measurements, the mean and error of this result will be proportional to $1/\sqrt{N}$ and take the exact value when $N \to \infty$.

3.1.2 Markov chains

The question that rises now, is how we can calculate the field configurations U_n, which behave according to the probability distribution given in Equation 3.3. We use the Markov chain, or Markov process, to construct a stochastic sequence of configurations that will eventually converge to an equilibrium distribution P(U).

$$U_0 \longrightarrow U_1 \longrightarrow U_2 \longrightarrow \cdots \,. \tag{3.4}$$

Each configuration U_n of the chain is generated subsequently. The chain starts from an initial position, U_0 and as it progresses, it visits points with higher probabilities (higher Boltzmann factors e^{-S}) more often. Any Markov process can be characterized by the conditional transition probability:

$$P(U_n = U'|U_{n-1} = U) = T(U|U')\,. \tag{3.5}$$

This shows that the state the system is transitioning to (U'), only depends on the one preceding it (U). The conditional probability is also normalized such that

$$0 \leq T(U|U') \leq 1\,,\ \sum_{U'} T(U'|U) = 1\,. \tag{3.6}$$

When the Markov chain has reached its equilibrium, the probability of transitioning into a state U', must be equal to the probability of transitioning out of it. This condition is described by the detailed balance equation, defined as

$$T(U'|U)P(U) = T(U|U')P(U') \tag{3.7}$$

We can employ the Metropolis algorithm [12] to generate configurations making use of the detailed balance condition, and the probability, $P(U) = e^{-S[U]}$. The steps are:

- We choose an initial candidate, U' , based on an initial selection probability, $T_0(U'|U)$, where U is a starting point for our chain.
- We either accept or discard the candidate, based on the acceptance probability, $T_A(U'|U)$
$$T_A(U'|U) = \min\left(1, \frac{T_0(U|U')e^{-S[U']}}{T_0(U'|U)e^{-S[U]}}\right)\,. \tag{3.8}$$
- Given that the transition is accepted, we use U' to evaluate whether the next generated candidate must be accepted or not. In the case where the transition is not accepted, we include the unchanged configuration in our measurements and repeat the first two steps for a different candidate.

3.2 Statistical analysis of simulated data

3.2.1 Analyzing correlated data

When analyzing data produced from a Monte Carlo simulation, one opts to derive the average value and its corresponding error, as a final value of the observable. There are two ways of doing this analysis, based on the type of data we have at hand. First, we assume that we have a set of values of a Markov sequence of Monte Carlo-generated configurations, $(x_1, x_2, ..., x_N)$. Each of the values corresponds to a random variable X_i. All of these random variables have the same expectation value and variance:

$$\langle X_i\rangle = \langle X\rangle, \sigma^2_{X_i} = \left\langle \left(X_i - \langle X_i\rangle\right)\right\rangle^2 = \sigma^2_X\,. \tag{3.9}$$

For X_i that are uncorrelated and $i \neq j$, $\langle X_iX_j\rangle = \langle X_i\rangle\langle X_j\rangle = \langle X\rangle$ also holds.
The estimators of the values we want to compute could be

$$\hat{X} = \frac{1}{N}\sum_{i=1}^{N} X_i\,,\ \hat{\sigma}^2_X = \frac{1}{N-1}\sum_{i=1}^{N}(X_i - \hat{X})^2\,. \tag{3.10}$$

It is easy to show, then, using Equation 3.9 that the mean and variance of the estimator are

$$\langle \hat{X} \rangle = \langle X \rangle, \quad \text{and} \quad \sigma^2_{\hat{X}} = \frac{1}{N}\sigma^2_X \,, \tag{3.11}$$

where we have also used the relation for uncorrelated X_i values. So, one can use Equation 3.10 to compute the expectation value and variance of data computed from Monte Carlo simulations, as

$$\hat{X} \pm \sigma \quad , \quad \text{where} \quad \sigma = \frac{\hat{\sigma}_X}{}.\sqrt{N} \tag{3.12}$$

Unfortunately, it is not often that the observables are not correlated. For data produced in a Monte-Carlo simulation, we need to take into account the autocorrelation, given be the auto-correlation function,

$$C_X\left(X_i, X_{i+t}\right) = \left\langle \left(X_i - \langle X_i \rangle\right)\left(X_{i+t} - \langle X_{i+t} \rangle\right) \right\rangle = \langle X_i X_{i+t} \rangle - \langle X_i \rangle \langle X_{i+t} \rangle \,, \tag{3.13}$$

which one must use to compute the autocorrelation time, τ, which affects the statistical error. In smaller data sizes, ($< 1000\tau$), where the autocorrelation time might not be easily calculated, we can use appropriate techniques to obtain the correlation in the data. In this work, we use the jackknife data blocking method, which is described below.

3.2.2 Jackknife resampling

Given that we wish to analyze fitted quantities, it is better and more correct to determine their means and errors over a set of data, rather than using error propagation. We do this by using the jackknife method for calculating the mean, error and correlation of our (fitted) quantities. This reduces the correlation and statistical error in our results. We start with a set of data, which we divide into blocks of size N. Each data point resembles an observable, α. We define the resampled m^{th} data point as

$$\bar{a}_m = \frac{1}{N-1}\sum_{i \neq m}^{N} a_i \; m = 1 \ldots N \,, \tag{3.14}$$

where we essentially calculate the mean value of the block after removing the m^{th} entry. These *resampled* data can now be used on any function f. The mean and error will become

$$\bar{F} = \frac{1}{N}\sum_{m=1}^{N} f(\bar{a}_m) \tag{3.15}$$

and

$$\sigma^2_F = \frac{N-1}{N}\sum_{m=1}^{N} (f(\bar{a}_m) - f(\bar{a})) \,, \tag{3.16}$$

with $\bar{\alpha}_m$ defined in Equation 3.14, and $\bar{\alpha}$ the general mean from Equation 3.10.
Lastly, in our analysis, we want to check that the estimated parameters of a fit, $\{p^{(i)}\}$, are the most compatible for each sample. This happens when the residual between the sample point and the function calculated using the estimated parameters becomes minimum, i.e., when $|f(\vec{x}_n, \{p^{(i)}\}) - \bar{\alpha}^{(i)}_n|$ is minimum. This is done by using the least squares method, and more specifically, by minimizing the χ^2 of the fit, which is given by

$$[\chi^{(i)}]^2 = \sum_{n=1}^{N}\sum_{m=1}^{N} \left(\bar{a}^{(i)}_n - f(\vec{x}_n, \{p^{(i)}\})\right) C^{-1}_{mn} \left(\bar{a}^{(i)}_m - f(\vec{x}_m, \{p^{(i)}\})\right) \,, \tag{3.17}$$

where C_{mn} is the covariance matrix between the data, defined as

$$C_{nm} = \frac{N-1}{N} \sum_{i=1}^{N} (\bar{a}_n^{(i)} - \bar{a}_n)(\bar{a}_m^{(i)} - \bar{a}_m) \,. \tag{3.18}$$

In the case for uncorrelated analysis, we only make use of the diagonal elements of C_{nm}. An indication that our data are well described by the fit comes from the reduced chi squared values of the fit, in which we divide Equation 3.17 by the degrees of freedom (d.o.f.) of the fit. A good value for the reduced χ^2 is ≈ 1.
Unfortunately, in our analysis, we often want to perform simultaneous analysis of ensembles with different sizes, which contribute more than one data point to our fit. In that case, we use an appropriate method to account for the correlations between the differences in the sample size, called *superjackknife*. As described in [13], using this process, we essentially create a "super-sample" of $N = \sum_i^M N_i$ super-jackknife blocks, where M is the total number of ensembles, with N_i samples each. The blocks are defined as follows: The first N_1 blocks consist of

$$\tilde{a}_{\alpha,k}^{(i)} = \begin{cases} \bar{a}_{\alpha,k}^{(i)} & : k = 1 \\ \bar{a}_{\alpha}^{(i)} & : k \neq 1 \end{cases} \text{, with } i = 1...N_1 \,, k = 1...M, \, \alpha = 1...n^{(i)} \,. \tag{3.19}$$

In the above expression, the notation $n^{(i)}$ represents the number of observables in the i^{th} ensemble. The index, k represents is the k^{th} super-jackknife block. The next N_2 blocks are defined as

$$\tilde{a}_{\alpha,k}^{(i)} = \begin{cases} \bar{a}_{\alpha,k+N_1}^{(i)} & : k = 2 \\ \bar{a}_{\alpha}^{(i)} & : k \neq 2 \end{cases} \text{, with } i = 1...N_2 \,, k = 1...M, \, \alpha = 1...n^{(i)} \tag{3.20}$$

and so on for the rest. The χ^2 equation, now can be generalized to

$$\chi_k^2 = \sum_{i=1}^{M} \sum_{\alpha=1}^{n^{(i)}} \sum_{\beta=1}^{n^{(i)}} \left(f(\vec{x}_\alpha, \{p^{(i)}\}) - \tilde{a}_{\alpha,k}^{(i)} \right) \left(f(\vec{x}_\beta, \{p^{(i)}\}) - \tilde{a}_{\beta,k}^{(i)} \right) (C^{(i)})_{\alpha\beta}^{-1} \,. \tag{3.21}$$

3.3 Hadron two-point correlation functions

The easiest fermion quantity to compute on the lattice is the mass of a hadron. The calculation of the mass spectrum and its agreement with experimental data prove the accuracy of lattice QCD and gives the motivation that it can hold for the calculation of other quantities as well.

Firstly, we must identify the hadron interpolators, $\mathcal{J}, \bar{\mathcal{J}}$, that will create the particle states we wish to analyze, with the corresponding quantum numbers. Then, we have to evaluate the Euclidean correlator of the interpolators $\mathcal{J}(n_t), \bar{\mathcal{J}}(0)$ at time slices $n_4 = n_t$ and $n_4 = 0$.

3.3.1 Meson interpolators

Mesons are bound states between a pair of quarks and anti-quarks, q and $\bar{q}$, generally different flavors $f_1$and f_2. The local interpolator used for such states is given by

$$\mathcal{J} = \bar{\psi}^{(f_1)}(n)\,\Gamma\,\psi^{(f_2)}(n)\,, \tag{3.22}$$

with Γ a monomial of gamma matrices. For the case where the two flavors differ, one has to construct appropriate combinations to preserve the flavor symmetries. We usually drop the flavor superscript and replace it with a unique symbol for each flavor: $u, \bar{u}, d, \bar{d}, s, \bar{s}, etc.$ The gamma matrices used for the most common meson interpolators are given in Table 2 For example, the iso-triplet interpolators of charged pions, which

State	J^{PC}	Γ	Particles
Scalar	0^{++}	$\mathbb{1}, \gamma_4$	$f_0, a_0, K_0^*, \cdots$
Pseudoscalar	0^{-+}	$\gamma_5, \gamma_4\gamma_5$	$\pi^{\pm}, \pi^0, \eta, K^{\pm}, K^0, \cdots$
Vector	1^{--}	$\gamma_i, \gamma_4\gamma_i$	$\rho^{\pm}, \rho^0, \omega, K^*, \phi, \cdots$
Axial vector	1^{++}	$\gamma_i\gamma_5$	$a_1, f_1, \cdots$
Tensor	1^{+-}	$\gamma_i\gamma_j$	$h_1, b_1, \cdots$

Table 2: Gamma matrices used for the most common meson interpolators, according to the quantum numbers of the particles, given in the second column.

are made up of u and d quarks, are constructed with combinations that return zero total spin, negative parity, isospin $I = 1$, $I_z = \pm 1$ and charge $Q = \pm e$ (we use summation convention)

$$\begin{aligned} \mathcal{J}_{\pi^+}(n) &= \bar{d}(n)\gamma_5 u(n) = \bar{d}(n)^c_\alpha\,(\gamma_5)_{\alpha,\beta}\,u(n)^c_\beta\,, \\ \mathcal{J}_{\pi^-}(n) &= \bar{u}(n)\gamma_5 d(n) = \bar{u}(n)^c_\alpha\,(\gamma_5)_{\alpha,\beta}\,d(n)^c_\beta\,. \end{aligned} \tag{3.23}$$

For the neutral pion, π^0, which returns $I_z = 0$, the iso-singlet interpolator is given by

$$\mathcal{J}_{\pi^0}(n) = \frac{1}{\sqrt{2}}\left(\bar{u}(n)\gamma_5 u(n) - \bar{d}(n)\gamma_5 d(n)\right)\,. \tag{3.24}$$

For the iso-singlet, $I = 0$ case of the $\eta-$meson, we get

$$\mathcal{J}_{\eta}(n) = \frac{1}{\sqrt{2}}\left(\bar{u}(n)\gamma_5 u(n) + \bar{d}(n)\gamma_5 d(n)\right)\,. \tag{3.25}$$

Interpolators for other meson states can be identified by a similar way.

To evaluate the correlators, we have to compute the Grassmann integrals of the expectation value between the fermions. We can utilize Wick's theorem for this part, and compute what is known as fermion contractions. It is important to note that only fermions with the same flavor can be contracted with each other. Thus, for the iso-triplet case, such as $\mathcal{J}_T = \bar{d}\Gamma u$, we find

$$\begin{aligned}
\langle \mathcal{J}_T(n)\bar{\mathcal{J}}_T(m)\rangle_F &= \langle \bar{d}(n)\Gamma u(n)\bar{u}(m)\Gamma d(m)\rangle_F \\
&= \Gamma_{\alpha_1\beta_1}\Gamma_{\alpha_2\beta_2}\langle \bar{d}(n)^{c_1}_{\alpha_1} u(n)^{c_1}_{\beta_1}\bar{u}(m)^{c_2}_{\alpha_2} d(m)^{c_2}_{\beta_2}\rangle_F \\
&= -\Gamma_{\alpha_1\beta_1}\Gamma_{\alpha_2\beta_2}\langle u(n)^{c_1}_{\beta_1}\bar{u}(m)^{c_2}_{\alpha_2}\rangle_u \langle d(m)^{c_2}_{\beta_2}\bar{d}(n)^{c_1}_{\alpha_1}\rangle_d \\
&= -\Gamma_{\alpha_1\beta_1}\Gamma_{\alpha_2\beta_2}\, D_u^{-1}(n|m)^{c_1c_2}_{\beta_1\alpha_2}\, D_d^{-1}(m|n)^{c_2c_1}_{\beta_2\alpha_1} \\
&= -\mathrm{tr}[\Gamma D_u^{-1}(n|m)\Gamma D_d^{-1}(m|n)]\,.
\end{aligned} \tag{3.26}$$

We interpret the final result as the propagation of the u(d) quark from point n(m) to point m(n). This combination is often referred as a connected piece.
On the other hand, for the iso-singlet state operator, such as $\mathcal{J}_S = (\bar{u}\Gamma u + \bar{d}\Gamma d)/\sqrt{2}$, we obtain

$$\begin{aligned}
\langle \mathcal{J}_S(n)\bar{\mathcal{J}}_S(m)\rangle_F = &-\frac{1}{2}\mathrm{tr}[\Gamma D_u^{-1}(n|m)\Gamma D_d^{-1}(m|n)] \\
&+\frac{1}{2}\mathrm{tr}[\Gamma D_u^{-1}(n|n)]\,\mathrm{tr}[\Gamma D_d^{-1}(m|m)] \\
&-\frac{1}{2}\mathrm{tr}[\Gamma D_d^{-1}(n|n)]\,\mathrm{tr}[\Gamma D_u^{-1}(m|m)] + u \leftrightarrow d\,.
\end{aligned} \tag{3.27}$$

The first line is similar to what we have obtained for the iso-triplet case. However, we also get quark propagators that transport quarks from point n(m), back to itself. These parts of the expectation value are called disconnected contributions. The schematic representation of connected and disconnected contributions is shown in Figure 2.

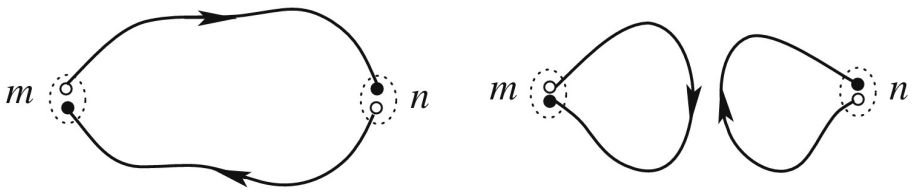

Figure 2: Schematic representation of connected contributions (left-hand side) and disconnected contributions (right-hand side) of a pion meson correlator [14].

3.3.2 Baryon interpolators

Baryons are made up of three quarks, such as protons and neutrons. Like the meson case, the interpolator we construct has to preserve the quantum numbers of the state we ae interested. For the proton, for example, the state we have is uud, with electric charge $Q = +e$, whereas for the neutron, we have udd, which is electrically neutral. For our discussion, though, electric charge does not play any role in QCD, and thus, the proton and neutron are manifested as different I_z components of a single state, referred to as the nucleon.
The simplest baryon interpolator for the nucleon is

$$J_N(n) = \epsilon^{abc} u(n)^a \left(u(n)^{b^T} C\gamma_5 d(n)^c \right) \tag{3.28}$$

The sum over the color indices using the Levi-Civita antisymmetric tensor ensures that the interpolator is gauge-invariant. The term in the parenthesis is a diquark, a combination of two quarks using the charge conjugation matrix, C and γ_5. It has total isospin $I = 0$ and spin $J = 0$ and we stress that it has no dynamical meaning. The full interpolator has spin $J = 1/2$, $I = 1/2$ and $I_z = +1/2$.
The parity of a nucleon is positive, thus the interpolator transforms as

$$\begin{aligned} \mathcal{J}_N^{\mathcal{P}}(\boldsymbol{n}, n_4) &= \epsilon^{abc} \gamma_4 u(-\boldsymbol{n}, n_4)^a u(-\boldsymbol{n}, n_4)^{b^T} \gamma_4^T C\gamma_5\gamma_4 d(-\boldsymbol{n}, n_4)^c \\ &= \epsilon^{abc} \gamma_4 u(-\boldsymbol{n}, n_4)^a u(-\boldsymbol{n}, n_4)^{b^T} C\gamma_5 d(-\boldsymbol{n}, n_4)^c = \gamma_4 \mathcal{J}_N(-\boldsymbol{n}, n_4)\,. \end{aligned} \tag{3.29}$$

The transformation of the spinor indices with γ_4 can be taken into account by considering the combination

$$\mathcal{J}_{N_\pm}(n) = \frac{1}{2}\left(\mathcal{J}_N(n) \pm \mathcal{J}_N^{\mathcal{P}}(n)\right) = \epsilon^{abc} P_\pm u(n)^a (u(n)^{b^T} C\gamma_5 d(n)^c)\,, \tag{3.30}$$

with $P_\pm = \frac{1}{2}(\mathbb{1} \pm \gamma_4)$. $\mathcal{J}_{N_+}$ fields have positive parity and represent a state with $P = +1$, whereas $\mathcal{J}_{N_-}$ fields have negative parity and represent a state with $P = -1$.
We can take the complex conjugate of the interpolating field and find the interpolator for creating a particle state

$$\overline{\mathcal{J}}_{N_\pm}(n) = \epsilon_{abc} \left(\bar{u}(n)^a C\gamma_5 \bar{d}(n)^{b^T} \right) \bar{u}(n)^c P_\pm\,. \tag{3.31}$$

After computing the fermion contraction on the two-point baryon function, we are left with

$$\begin{aligned} &\langle \mathcal{J}_{N_\pm}(n)_\alpha \bar{\mathcal{J}}_{N_\pm}(m)_\alpha \rangle_F = -\langle \bar{\mathcal{J}}_{N_\pm}(m)_\alpha \mathcal{J}_{N_\pm}(n)_\alpha \rangle_F \\ &= -\left\langle \epsilon^{abc}\epsilon^{a'b'c'} \left(\bar{u}^a(m) C\gamma_5 (\bar{d}^b(m))^T\right) \bar{u}^c(m) P_\pm u^{c'}(n) \left((u^{a'}(n))^T C\gamma_5 d^{b'}(n) \right) \right\rangle_F \\ &= \epsilon^{abc}\epsilon^{a'b'c'} (C\gamma_5)_{\beta\delta} (C\gamma_5)_{\alpha\gamma} (P_\pm)_{\rho\sigma} D_d^{-1}(n|m)^{b'b}_{\delta\beta} \times \\ &\quad \left(D_u^{-1}(n|m)^{a'a}_{\alpha'\alpha} D_u^{-1}(n|m)^{c'c}_{\gamma'\gamma} - D_u^{-1}(n|m)^{c'a}_{\gamma'\alpha} D_u^{-1}(n|m)^{a'c}_{\alpha'\gamma} \right)\,. \end{aligned} \tag{3.32}$$

It is therefore shown that for the baryon states, only connected parts contribute to the two-point function.

3.3.3 Momentum projection

The definition we give to the hadron states has to have definite spatial momentum $\mathbf{p}$. We are led to define

$$\widetilde{\mathcal{J}}(\mathbf{p}, n_t) = \frac{1}{\sqrt{|\Lambda_3|}} \sum_{n \in \Lambda_3} \mathcal{J}(\mathbf{n}, n_t) e^{-ia\mathbf{n}\cdot\mathbf{p}} \,. \tag{3.33}$$

The interpolator $\widetilde{\mathcal{J}}(\mathbf{p}, n_t)$ is projected to definite spatial momentum and is located at a single time slice n_t. It is sufficient to only project one of the two interpolators to definite momentum. The source operator, $\bar{\mathcal{J}}(\mathbf{0}, 0)$ can still be in real space and placed at the origin. We find the final formula for the hadron correlators to be

$$\begin{aligned} \langle \widetilde{\mathcal{J}}(\mathbf{p}, n_t) \bar{\mathcal{J}}(\mathbf{0}, 0) \rangle &= \frac{1}{\sqrt{|\Lambda_3|}} \sum_{n \in \Lambda_3} e^{-ia\mathbf{n}\cdot\mathbf{p}} \langle \mathcal{J}(\mathbf{n}, n_t) \bar{\mathcal{J}}(\mathbf{0}, 0) \rangle \\ &= A e^{-a n_t E(\mathbf{p})} (1 + \mathcal{O}(e^{-a n_t \Delta E})) \,, \end{aligned} \tag{3.34}$$

where the energy $E(\mathbf{p})$ is related to the hadron mass by the relativistic dispersion relation, which in units where $c = 1$ reads

$$E(\mathbf{p}) = \sqrt{m_H^2 + \mathbf{p}^2}(1 + \mathcal{O}(ap)) \overset{(\mathbf{p}=0)}{=} m_H \tag{3.35}$$

To obtain results for any product of correlators $\mathcal{O}$ we evaluate

$$\langle \mathcal{O} \rangle = \langle \langle \mathcal{O} \rangle_F \rangle_G = \frac{1}{Z} \int \mathcal{D}[U] e^{-S_G[U]} \mathcal{D}[\psi, \bar{\psi}] e^{-S_F[\psi, \bar{\psi}, U]} \mathcal{O}[\psi, \bar{\psi}, U] \,. \tag{3.36}$$

For the case of the nucleon propagator, for example, this integral becomes

$$\langle \mathcal{J}_{N_\pm}(n) \bar{\mathcal{J}}_{N_\pm}(m) \rangle_F = \frac{1}{Z} \int \mathcal{D}[U] e^{-S_G[U]} \det[D_u[U]] \det[D_d[U]] \langle \mathcal{J}_{N_\pm}(n) \bar{\mathcal{J}}_{N_\pm}(m) \rangle_F \,. \tag{3.37}$$

We need to perform Monte Carlo simulations using as the distribution weight for the fermion fields

$$\frac{1}{Z} e^{-S_G[U]} \det[D_u[U]] \det[D_d[U]] \,. \tag{3.38}$$

One has to be careful in this step, as the computation of the Dirac determinant is not an easy task. The Dirac matrix contains $12|\Lambda|$ rows and columns, with Λ the number of lattice sites. Its dimension is of the order of millions.

3.4 Hadron three-point correlation functions

Our previous discussion has only included the simplest correlator, the two-point function, from which one can extract the mass of a particle. For more interesting quantities, such as the hadron charge radii, hadron decay amplitudes and form factors, one has to compute three-point functions.

A three-point function is given in its general form by

$$C^\mu(x_s; x_{ins}; 0) = \langle \Omega | \mathcal{J}(x_s) \mathcal{O}^\mu(x_{ins}) \bar{\mathcal{J}}(0) | \Omega \rangle \,, \tag{3.39}$$

where x_s is the sink point and x_{ins} is the point where the operator $\mathcal{O}^\mu$ is inserted. This is connected to the lattice interpretation by setting $x = an$.

Following the same steps we did with the two-point function, we perform momentum projection by two Fourier transformations over $\vec{x}_s$ and $\vec{x}_{ins}$. Due to momentum conservation, the momentum at the source is automatically fixed from the momentum at the insertion and sink. Thus, after the Fourier transformation we obtain

$$C^{\mu}(\vec{p}', t_s; \vec{p}_1, t_{ins}) = \sum_{\vec{x}_s, \vec{x}_{ins}} C^{\mu}(\vec{x}_s, t_s; \vec{x}_{ins}, t_{ins}) e^{-i\vec{x}_s \cdot \vec{p}'} \, e^{+i\vec{x}_{ins} \cdot \vec{p}_1} \, . \tag{3.40}$$

We can use the Heisenberg picture to insert the Hamiltonian and momentum operators $\mathcal{H}$ and $\vec{\mathcal{P}}$. The format now becomes

$$\begin{aligned} C^{\mu}(\vec{p}', t_s; \vec{p}_1, t_{ins}) = & \sum_{\vec{x}_s, \vec{x}_{ins}} e^{-i\vec{x}_s \cdot \vec{p}'} \, e^{+i\vec{x}_{ins} \cdot \vec{p}_1} \times \\ & \langle \Omega | \mathcal{J}(\vec{0}, 0) e^{-\mathcal{H} t_s} e^{i\vec{x}_s \cdot \vec{\mathcal{P}}} e^{-i\vec{x}_{ins} \cdot \vec{\mathcal{P}}} e^{\mathcal{H} t_{ins}} \mathcal{O}^{\mu} e^{-\mathcal{H} t_{ins}} e^{i\vec{x}_{ins} \cdot \vec{\mathcal{P}}} \bar{\mathcal{J}}(\vec{0}, 0) | \Omega \rangle \, . \end{aligned} \tag{3.41}$$

We now proceed to insert complete states of energy and momentum eigenstates $|n, \vec{k}\,\rangle$, $|n', \vec{k}'\,\rangle$. The correlator takes the form

$$\begin{aligned} C^{\mu}(\vec{p}', t_s; \vec{p}_1, t_{ins}) = & \sum_{\vec{x}_s, \vec{x}_{ins}} \sum_{n, n'} \sum_{\vec{k}, \vec{k}'} \langle \Omega | \mathcal{J} | n', \vec{k}' \rangle \langle n, \vec{k} | \bar{\mathcal{J}} | \Omega \rangle \times \\ & e^{-i\vec{x}_s \cdot (\vec{p}' - \vec{k}')} \, e^{-i\vec{x}_{ins} \cdot (\vec{k}' - \vec{k} - \vec{p}_1)} \, e^{-E_{n'}(\vec{k}')(t_s - t_{ins})} \, e^{-E_n(\vec{k}) t_{ins}} \, \langle n', \vec{k}' | \mathcal{O}^{\mu} | n, \vec{k} \rangle \, . \end{aligned} \tag{3.42}$$

Taking the limit at large time, where $(t_s - t_{ins}) \to \infty$ and $t_{ins} \to \infty$, the three-point function becomes

$$\begin{aligned} C^{\mu}(\vec{p}', t_s; \vec{p}_1, t_{ins}) = & \langle \Omega | \mathcal{J} | H(\vec{p}') \rangle \, \langle H(\vec{p}_1) | \bar{\mathcal{J}} | \Omega \rangle \times \\ & \langle H(\vec{p}') | \mathcal{O}^{\mu} | H(\vec{p}' - \vec{p}_1) \rangle \, e^{-E(\vec{p}')(t_s - t_{ins})} e^{-E(\vec{p}_1 t_{ins})} \, . \end{aligned} \tag{3.43}$$

Similarly, the two-point function would become

$$C(\vec{p}, t_s) = \langle \Omega | \mathcal{J} | H(\vec{p}) \rangle \, \langle H(\vec{p}) | \bar{\mathcal{J}} | \Omega \rangle e^{-E(\vec{p}) t_s} \, , \tag{3.44}$$

with $H(\vec{p})$ the eigenstates of the hadron. We are interested in evaluating the matrix element $\langle H(\vec{p}') | \mathcal{O}^{\mu} | H(\vec{p}' - \vec{p}_1) \rangle$, thus, we compute appropriate ratios between two- and three- point functions, that isolate it from the exponential terms.

3.5 Nucleon three-point functions

To compute the three-point function for the nucleon we use the interpolating field

$$\mathcal{J}^N_{\alpha}(x) = \epsilon^{abc} u^a_{\alpha}(x) \left(u^b_{\mu}(x) (C\gamma_5)_{\mu\nu} \, d^c_{\nu}(x) \right) \, . \tag{3.45}$$

The insertion operator is given by

$$\mathcal{G}^{\rho}(x_{ins}) = \bar{u}^f_{\kappa}(x_{ins}) (\gamma_{\rho})_{\kappa\lambda} \, u^f_{\lambda}(x_{ins}) \, . \tag{3.46}$$

The three-point function equation reads

$$\begin{aligned} C^{\rho}(x_s; x_{ins}; 0) = & \langle \Omega | \mathcal{J}(x_s) \mathcal{G}^{\rho}(x_{ins}) \bar{\mathcal{J}}(0) | \Omega \rangle \\ = & \langle \Omega | \epsilon^{abc} u^a_{\alpha}(x_s) \left(u^b_{\mu}(x_s) (C\gamma_5)_{\mu\nu} \, d^c_{\nu}(x_s) \right) \times \\ & \bar{u}^f_{\kappa}(x_{ins}) \, (\gamma_{\rho})_{\kappa\lambda} \, u^f_{\lambda}(x_{ins}) \times \\ & \epsilon^{a'b'c'} \bar{u}^{c'}_{\alpha'}(0) \bar{d}^{b'}_{\nu'}(0) \, (\bar{C}\bar{\gamma}_5)_{\nu'\mu'} \bar{u}^{a'}_{\mu'}(0) | \Omega \rangle \, . \end{aligned} \tag{3.47}$$

Computing the fermion contractions we derive the final expressions

$$
\begin{aligned}
C^{\rho}(x_s;x_{ins};0) = \epsilon^{abc}\epsilon^{a'b'c'}\, \left[C\gamma_5 D_d^{-1}(x_s|0)\bar{C}\bar{\gamma}_5\right]^{b'b}_{\mu\nu} \times \\
\Bigg[\left[D_u^{-1}(x_s|x_{ins})\gamma_\rho\, D_u^{-1}(x_{ins}|0)\right]^{aa'}_{\mu\mu'} D_u^{-1}(x_s|0)^{cc'}_{\alpha\alpha'} \\
- \left[D_u^{-1}(x_s|x_{ins})\gamma_\rho\, D_u^{-1}(x_{ins}|0)\right]^{ac'}_{\mu\alpha'} D_u^{-1}(x_s|0)^{ca'}_{\mu\mu'} \\
+ \left[D_u^{-1}(x_s|x_{ins})\gamma_\rho\, D_u^{-1}(x_{ins}|0)\right]^{cc'}_{\alpha\alpha'} D_u^{-1}(x_s|0)^{aa'}_{\mu\mu'} \\
- \left[D_u^{-1}(x_s|x_{ins})\gamma_\rho\, D_u^{-1}(x_{ins}|0)\right]^{ca'}_{\alpha\mu'} D_u^{-1}(x_s|0)^{ac'}_{\mu\alpha'} \\
+ \Big\{ \left[D_u^{-1}(x_{ins}|x_{ins})\gamma_\rho\right]^{ff}_{\lambda\lambda} \times \\
\left(D_u^{-1}(x_s|0)^{cc'}_{\alpha\alpha'} D_u^{-1}(x_s|0)^{\alpha\alpha'}_{\mu\mu'} - D_u^{-1}(x_s|0)^{ac'}_{\mu\alpha'} D_u^{-1}(x_s|0)^{ca'}_{\alpha\mu'} \right) \Big\} \Bigg] .
\end{aligned}
\tag{3.48}
$$

The last two lines in the curly brackets in the above expression represent the disconnected loop contributions, while the rest are the connected pieces of the three-point function.

4 Nucleon Generalized Form Factors

The nucleon Generalized Form Factors (GFFs), evaluated from the EMT matrix elements, give the spin properties of the nucleon. In this chapter we give the methods to extract and analyze them using numerical simulations, as previously discussed. Finally, we show our results and discuss them in comparison with other studies.

4.1 Matrix element decomposition

The energy-momentum tensor (EMT) operator is given by

$$T^{\mu\nu} \equiv \bar{q}(x)\gamma^{\{\mu} i \overleftrightarrow{D}^{\nu\}} q(x) \tag{4.1}$$

For the isovector combination we have

$$T^{\mu\nu} = \bar{u}(x)\gamma^{\{\mu} i \overleftrightarrow{D}^{\nu\}} u(x) \; - \; \bar{d}(x)\gamma^{\{\mu} i \overleftrightarrow{D}^{\nu\}} d(x)\,, \tag{4.2}$$

whereas for the isoscalar combination we have

$$T^{\mu\nu} = \bar{u}(x)\gamma^{\{\mu} i \overleftrightarrow{D}^{\nu\}} u(x) \; + \; \bar{d}(x)\gamma^{\{\mu} i \overleftrightarrow{D}^{\nu\}} d(x)\,, \tag{4.3}$$

with $u(x)$ and $d(x)$ the up- and down- quark fermion fields, respectively. The nucleon matrix elements of the EMT, are decomposed into three generalized form factors (GFFs), namely $A_{20}(q^2), B_{20}(q^2)$ and $C_{20}(q^2)$. They are expressed in Minkowski space as [15]

$$\begin{aligned}\langle N\left(p',s'\right)|T^{\mu\nu;q,g}|N\left(p,s\right)\rangle = \bar{u}_N\left(p',s'\right)\Bigg[A_{20}^{q,g}(q^2)\gamma^{\{\mu}P^{\nu\}} + B_{20}^{q,g}(q^2)\frac{i\sigma^{\{\mu\rho}q_\rho P^{\nu\}}}{2m_N} \\ + C_{20}^{q,g}(q^2)\frac{q^{\{\mu}q^{\nu\}}}{m_N}\Bigg] u_N(p,s)\,.\end{aligned} \tag{4.4}$$

where u_N are the nucleon spinors, with initial and final momentum and spin, $\{p,s\}$ and $\{p',s'\}$ respectively. P and q are defined such that $P = \frac{p+p'}{2}$ is the total momentum and $q = p - p'$ is the total momentum transfer.
In the case of zero momentum transfer, i.e. $p = p'$, Equation 4.4 reduces to

$$\langle N\left(p,s'\right)|T^{\mu\nu;q,g}|N\left(p,s\right)\rangle = \frac{1}{2}A_{20}^{q,g}(0)\bar{u}_N\left(p,s'\right)\gamma^{\{\mu}p^{\nu\}}u_N\left(p,s\right)\,, \tag{4.5}$$

where $A_{20}^{q,g}(0) = \langle x\rangle^{q,g}$, the quark and gluon average momentum fraction. We are therefore unable to determine the rest of the form factors in zero momentum transfer, since the kinematic factors in front of them disappear. The solution we resolve to, is to compute B_{20} and C_{20} at finite momentum transfer and extrapolate to $Q^2 = 0$, using an appropriate fit Ansatz. In order to be able to do that, however, one has to isolate B_{20} and C_{20} from the decomposition in Equation 4.4. We construct appropriate ratios of two- and three-point functions in Euclidean space, with quantum numbers corresponding to the nucleon, from which we can, using singular value decomposition isolate each form factor.

We use the trace of the projector and compute the two-point functions as

$$C\left(\Gamma_0,\vec{p};t,t_0\right) = \sum_{\vec{x}_s} e^{-i(\vec{x}_s-\vec{x}_0)\cdot\vec{p}} \times \mathrm{Tr}\left[\Gamma_0\langle\mathcal{J}_N(t_s,\vec{x}_s)\bar{\mathcal{J}}_N(t_0,\vec{x}_0)\rangle\right]\,. \tag{4.6}$$

Similarly, the three-point function is given by

$$C^{\mu\nu}(\Gamma_\rho, \vec{q}, \vec{p}'; t_s, t_{ins}, t_0) = \sum_{\vec{x}_{ins}, \vec{x}_s} e^{i(\vec{x}_{ins}-\vec{x}_0)\cdot\vec{q}} e^{-i(\vec{x}_s-\vec{x}_0)\cdot\vec{p}'} \times \\ \mathrm{Tr}\left[\Gamma_\rho \langle \mathcal{J}_N(t_s, \vec{x}_s) \mathcal{O}^{\mu\nu}(t_{ins}, \vec{x}_{ins}) \bar{\mathcal{J}}_N(t_0, \vec{x}_0)\rangle\right] , \tag{4.7}$$

where $\mathcal{O}^{\mu\nu}$ represents the energy-momentum tensor, x_0, x_{ins} and x_s are the initial lattice site, where the states are created, referred to as source position, insertion lattice site, where the operator probes at the quarks and gluons, referred to as insertion point and the site at which the states are annihilated, referred to as sink position, respectively. Lastly, we consider the projectors acting on the spin indices: $\Gamma_0 = \frac{1}{2}(1+\gamma_0)$ and $\Gamma_\rho = i\Gamma_0\gamma_5\gamma_\rho$, as we take the non relativistic representation of γ_μ.
The interpolating field we use is

$$\mathcal{J}_N(t, \vec{x}) = \epsilon_{abc} u_a(x) \left[u_b^T(x) \mathcal{C}\gamma_5 d_c(x)\right] , \tag{4.8}$$

where $u(x)$, $d(x)$ are the up and down quark fields and $\mathcal{C}$ is the charge conjugation matrix. This field does not only create the nucleon ground state, but excited nucleon states as well, which include multi-particle states. Since we are interested in analyzing the nucleon state, we employ Gaussian smearing [16],[17] on the quark fields, in order to increase the overlap between the field and the ground states of the nucleon. The smeared quark fields are given by

$$q_{\mathrm{smeared}}(t, \vec{x}) = \sum_{\vec{y}} \left(1 + a_G H\right)^{n_G} q(t, \vec{x}) , \tag{4.9}$$

with H the hopping matrix

$$H(\vec{x}, \vec{y}, U(t)) = \sum_{i=1}^{3} \left[U_i(x)\delta_{x,y-\hat{i}} + U_i^\dagger(x-\hat{i})\delta_{x,y+\hat{i}}\right] . \tag{4.10}$$

The spectral decomposition of the two- and three- point functions are given by

$$C(\Gamma_0, \vec{p}; t, t_0) = \sum_{i=0}^{\infty} c_i(\vec{p}) e^{-E_i(\vec{p})t_s} \quad \text{and} \\ C^{\mu\nu}(\Gamma_\rho, \vec{p'}, \vec{p}; t_s, t_{ins}) = \sum_{i,j=0}^{\infty} \mathcal{A}_{i,j}^{\mu\nu}(\Gamma_\rho, \vec{p'}, \vec{p})\, e^{-E_i(\vec{p}')(t_s-t_{ins}) - E_j(\vec{p})t_{ins}} . \tag{4.11}$$

The coefficients c_i are the overlap terms of the two-point function, given by

$$c_i(\vec{p}) = \mathrm{tr}\left[\Gamma_0 \langle\Omega|\mathcal{J}_N|N_i(\vec{p})\rangle \langle N_i(\vec{p})|\mathcal{J}_N^\dagger|\Omega\rangle\right] \tag{4.12}$$

and $\mathcal{A}_{i,j}^{\mu\nu}$, are respectfully given by

$$\mathcal{A}_{i,j}^{\mu\nu}(\Gamma_\rho, \vec{p'}, \vec{p}) = \mathrm{tr}\left[\Gamma_\rho \langle\Omega|\mathcal{J}_N|N_i(\vec{p}')\rangle \langle N_i(\vec{p}')|\mathcal{O}^{\mu\nu}|N_j(\vec{p})\rangle \langle N_j(\vec{p})|\mathcal{J}_N^\dagger|\Omega\rangle\right] . \tag{4.13}$$

The desired matrix element is given by $\langle N_i(\vec{p}')|\mathcal{O}^{\mu\nu}|N_j(\vec{p})\rangle$.

In order to benefit from the correlations between two- and three- point functions, we construct an appropriate ratio between the two, which in large Euclidean time limit

cancels the time dependence, and the nucleon ground state dominates. In our case, the choice we opt for is

$$R^{\mu\nu}(\Gamma_\rho, \vec{p}', \vec{p}; t_s, t_{ins}) = \frac{C^{\mu\nu}(\Gamma_\rho, \vec{p}', \vec{p}; t_s, t_{ins})}{C(\Gamma_0, \vec{p}'; t_s)} \times \sqrt{\frac{C(\Gamma_0, \vec{p}; t_s - t_{ins})C(\Gamma_0, \vec{p}'; t_{ins})C(\Gamma_0, \vec{p}'; t_s)}{C(\Gamma_0, \vec{p}'; t_s - t_{ins})C(\Gamma_0, \vec{p}; t_{ins})C(\Gamma_0, \vec{p}; t_s)}}\,. \tag{4.14}$$

As stated above, this ratio should, at $t_s - t_{ins} \gg \alpha$ and $t_{ins} \gg \alpha$, with α the lattice spacing, return:

$$R^{\mu\nu}(\Gamma_\rho; \vec{p}', \vec{p}, t_s, t_{ins}) \xrightarrow[t_{ins}\gg\alpha]{t_s - t_{ins}\gg\alpha} \Pi^{\mu\nu}(\Gamma_\rho; \vec{p}', \vec{p}) = \frac{\mathcal{A}^{\mu\nu}_{0,0}}{\sqrt{c_0(\vec{p})c_0(\vec{p}')}}\,, \tag{4.15}$$

which yields the nucleon matrix element, independent of time. In our work we sustain to keeping the momentum sink at zero, i.e., we fix $\vec{p}' = \vec{0}$.
Returning back to the extraction of the form factors, in order to isolate $A_{20}(q^2; t_s, t_{ins})$, $B_{20}(q^2; t_s, t_{ins})$ and $C_{20}(q^2; t_s, t_{ins})$, we first minimize the equation

$$\chi^2 = \sum_{\rho,\mu,\nu} \sum_{\vec{p}', \vec{p} \in Q^2} \left[\frac{\mathcal{G}^{\mu\nu}(\Gamma_\rho, \vec{p}', \vec{p}) F(q^2; ts, t_{ins}) - R^{\mu\nu}(\Gamma_\rho, \vec{p}', \vec{p}; t_s, t_{ins})}{w^{\mu\nu}(\Gamma_\rho, \vec{p}', \vec{p}; t_s, t_{ins})} \right], \tag{4.16}$$

where R is the ratio as defined in Equation 4.14, w is the statistical error, $\mathcal{G}$ are the kinematical coefficients of the form factors, as defined in Appendix D and, lastly, F is the vector that gives the three form factors:

$$F(q^2; t_s, t_{ins}) = \begin{pmatrix} A_{20}(q^2; t_s, t_{ins}) \\ B_{20}(q^2; t_s, t_{ins}) \\ C_{20}(q^2; t_s, t_{ins}) \end{pmatrix}. \tag{4.17}$$

The time dependence appearing in Equation 4.17 comes from excited state contributions, which we will be analyzing using methods described below.
Instead of minimizing Equation 4.16, we can show that Equation 4.17 can be extracted from

$$F = V^\dagger \Sigma^{-1} U^\dagger \widetilde{R}\,, \tag{4.18}$$

where

$$\begin{aligned} \widetilde{R}^{\mu\nu}(\Gamma_\rho, \vec{p}', \vec{p}) &= \left[w^{\mu\nu}(\Gamma_\rho, \vec{p}', \vec{p})\right]^{-1} R^{\mu\nu}(\Gamma_\rho, \vec{p}', \vec{p}), \\ \widetilde{\mathcal{G}}^{\mu\nu}(\Gamma_\rho, \vec{p}', \vec{p}) &= \left[w^{\mu\nu}(\Gamma_\rho, \vec{p}', \vec{p})\right]^{-1} \mathcal{G}^{\mu\nu}(\Gamma_\rho, \vec{p}', \vec{p}), \\ \widetilde{\mathcal{G}} &= U \Sigma V\,. \end{aligned} \tag{4.19}$$

In the last line of Equation 4.19 we compute the Singular Value Decomposition (SVD) of $\widetilde{\mathcal{G}}$: U is a hermitian $N \times N$ matrix, with N being the number of nonzero combinations of μ, ν, ρ that contribute to the same Q^2, Σ an $N \times 3$ pseudo-diagonal matrix of the singular values of $\widetilde{\mathcal{G}}$ and V a hermitian 3×3 matrix [18].

4.2 Fitting procedure

We employ two- and three- point functions from three different $N_f = 2+1+1$ ensembles, generated by the *Extended Twisted Mass Collaboration (ETMC)*,the characteristics of which are shown in Table 3.

Table 3: Simulation parameters used for the three $N_f = 2 + 1 + 1$ ensembles of this work. The first column gives the name of the ensemble, α is the lattice spacing, V is the lattice volume in lattice units, L is the spatial lattice length in physical units, m_π is the pion mass and m_N is the nucleon mass, both in GeV. The data was taken from [19].

Ensemble	Abbreviation	$\alpha\,[fm]$	V	$L\,[fm]$	m_π [GeV]	m_N [GeV]
cB211.072.64	cB64	0.07951	$64^3 \times 128$	5.08864	0.14040	0.3810
cC211.060.80	cC80	0.06816	$80^3 \times 160$	5.4528	0.13605	0.3246
cD211.054.96	cD96	0.05688	$96^3 \times 192$	5.46048	0.14101	0.27261

4.2.1 Fitting methods

To construct the ratios of Equation 4.14, we use three- and two- point functions with the same statistics, to benefit from the correlations between them. For the independent two-point function fits we make use of the two-point function with the higher statistics. Upon extracting the ratios representing each form factor, the procedure for the analysis is as follows:

- Two-state method: In order to be able to factor out the excited states, we expand the two- and three- point functions of Equation 4.11 up-to $i, j = 1$, considering two states (the ground and first excited) to our fitting model:

$$C(\vec{p}, t_s) = c_0(\vec{p})e^{-E_0(\vec{p})t_s} + c_1(\vec{p})e^{-E_1(\vec{p})} \tag{4.20}$$

  for the two-point function and

$$\begin{aligned} C^{\mu\nu}(\Gamma_\rho, \vec{p}', \vec{p}, t_s, t_{ins}) = &\mathcal{A}^{\mu\nu}_{0,0}(\Gamma_\rho, \vec{p}', \vec{p})e^{-E_0(\vec{p}')(t_s - t_{ins}) - E_0(\vec{p})t_{ins}} \\ &+ \mathcal{A}^{\mu\nu}_{0,1}(\Gamma_\rho, \vec{p}', \vec{p})e^{-E_0(\vec{p}')(t_s - t_{ins}) - E_1(\vec{p})t_{ins}} \\ &+ \mathcal{A}^{\mu\nu}_{1,0}(\Gamma_\rho, \vec{p}', \vec{p})e^{-E_1(\vec{p}')(t_s - t_{ins}) - E_0(\vec{p})t_{ins}} \\ &+ \mathcal{A}^{\mu\nu}_{1,1}(\Gamma_\rho, \vec{p}', \vec{p})e^{-E_1(\vec{p}')(t_s - t_{ins}) - E_1(\vec{p})t_{ins}} \end{aligned} \tag{4.21}$$

  for the three-point function.
  The coefficients $c_0(\vec{p})$ and $c_1(\vec{p})$ represent the overlaps of the ground and first excited state with the interpolating field for the two-point function and $\mathcal{A}^{\mu\nu}_{i,j}$ are the matrix elements of the i,j states multiplied by the corresponding parameters. $E_0(\vec{p})$ and $E_1(\vec{p})$ are the energies of the ground and first excited state at momentum $\vec{p}$. In the case of non-zero momentum transfer, $\mathcal{A}^{\mu\nu}_{0,1} \neq \mathcal{A}^{\mu\nu}_{1,0}$, whereas for $\vec{p} = \vec{p}' = \vec{0}$, the two are the same.

- Plateau method: We write the ratio of Equation 4.14 as a sum of the ground and excited states of the nucleon, i.e.,

$$R^{\mu\nu} = \Pi^{\mu\nu}(\Gamma_\rho; \vec{p}', \vec{p}) + \mathcal{O}(e^{-\Delta E(t_s - t_{ins})}) + \mathcal{O}(e^{-\Delta E t_{ins}}) + \cdots, \tag{4.22}$$

  where the first term is the time-independent nucleon matrix element that we are looking for. The rest terms describe the excited states and are suppressed. We therefore look for t_{ins} for which we can neglect the excited state contributions.
  More specifically, depending on the parameter we wish to extract, we vary the range of t_s or t_{ins}, as follows:

- Effective mass two-state fits: We perform two-state fits on the effective mass, to benefit from the correlations between the ratios of $\frac{C(\vec{p},t_s+1)}{C(\vec{p},t_s)}$. We vary the range of t_s used to fit the two-point function with full statistics to the two-state form of the effective mass,

$$M_{eff} = -\ln\left[\frac{C(\vec{p},t_s+1)}{C(\vec{p},t_s)}\right] = m_N + \ln\left[\frac{1+\frac{c_1(\vec{p})}{c_0(\vec{p})}e^{-\Delta E t_s}}{1+\frac{c_1(\vec{p})}{c_0(\vec{p})}e^{-\Delta E(t_s+1)}}\right]. \tag{4.23}$$

- Ratio two-state fits: We make use of the two-state form of Equation 4.11 on Equation 4.14 and fit to extract the coefficients and matrix elements of the two- and three- point functions. We perform simultaneous fits of the ratios with $t_s \geq t_s^{low}$, where we vary t_s^{low} to check the convergence of the extracted nucleon matrix element. We vary the insertion time slices t_{ins}, so that $t_{ins} \in [\tau, t_s - \tau]$, where $\tau \in [2, 3]$.

- Ratio plateau fits: We fit the ratios for each t_s to a plateau, varying the number of insertion time slices, t_{ins}, so that $t_{ins} \in [2+\tau, t_s - \tau - 2]$, where $\tau \in [0, t_s/2 - 1]$, for the various t_s values.

4.3 Model averaging

Since we adopt the several fitting methods for each jackknife block, we get various parameters. We average the results from all blocks using the Akaike Information Criterion (AIC) [20],[21]. Essentially, to each fit, i, we assign a weight, w_i defined as

$$\log(w_i) = -\frac{\chi_i^2}{2} + N_{\text{dof},i}\,, \tag{4.24}$$

where $N_{\text{dof}} = N_{\text{data}} - N_{\text{params}}$, is the number of degrees of freedom, and χ^2 is defined as in Equation 3.17. From the weights we define the normalized probability for each fit i, as

$$p_i = \frac{w_i}{Z} \text{ with } Z = \sum_i w_i\,. \tag{4.25}$$

The model-averaged value of an observable, $\mathcal{O}$ is calculated as

$$\begin{aligned} \langle\mathcal{O}\rangle &= \text{mean(error)} \\ \text{with mean} &= \sum_i \bar{\mathcal{O}}_i p_i \\ \text{and error}^2 &= \sum_i (\sigma_i^2 + \bar{\mathcal{O}}_i^2) p_i - \text{mean}^2\,, \end{aligned} \tag{4.26}$$

where $\bar{\mathcal{O}}_i$ and σ_i are the central value and error of the observable on the i^{th} fit.

4.4 Excited state analysis

For our results to relate to physical observables, we have to renormalize them. We note that since we have only analyzed the connected contributions of our data, there are no mixing parameters involved in the renormalization process. This leads us to calculate only two components of renormalization: $Z^{\mu=\nu}$, for the case where $\mu = \nu$ and $Z^{\mu\neq\nu}$, which corresponds to $\mu \neq \nu$. The values for all ensembles are given in Table 4 below.

Table 4: Renormalization constants used for the three ensembles analyzed in this work.[22]

Ensemble	$Z^{\mu=\nu}$	$Z^{\mu\neq\nu}$
cB64	1.1167(4)	1.1262(4)
cC80	1.1460(2)	1.1573(3)
cD96	1.1807(2)	1.1930(2)

4.4.1 Effective mass fits

We first perform the effective mass fits, in order to extract the energy decomposition for each ensemble, at zero and finite momentum transfer. More specifically, we extract the nucleon mass, m_N, the overlapping factor $\frac{c_1(\vec{p})}{c_0(\vec{p})}$, and $\Delta E(\vec{p}) = E_1(\vec{p}) - E_0(\vec{p})$, where we compute $E_0(\vec{p})$ using the dispersion relation and the nucleon mass: $E_0(\vec{p}) = \sqrt{m_N^2 + \vec{p}^2}$.

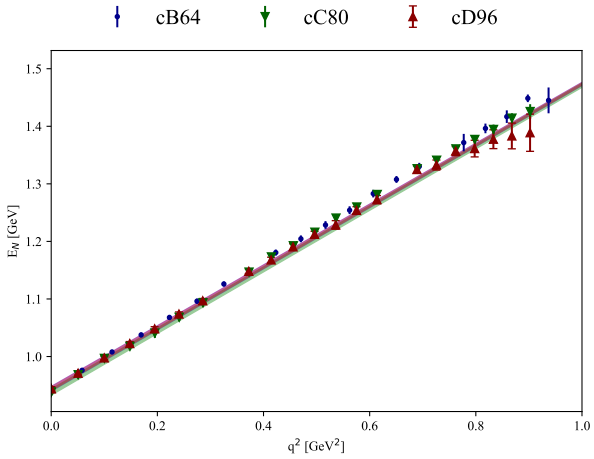

Figure 3: The points represent the nucleon energy, E_N in GeV, as extracted from the effective mass two-state fits for each ensemble. The corresponding bands show the dispersion relation $E_N(q^2) = \sqrt{m_N^2 + \vec{q}^2}$. The data are plotted as a function of q^2 in GeV^2. In the header of the figure we give the symbols used to distinguish between the three ensembles.

4.4.2 Extracting the GFFs: $\mathbf{A_{20}}(Q^2)$

As previously mentioned, we can begin analyzing the isoscalar and isovector contributions of $A_{20}(Q^2)$ at zero momentum transfer. This will yield the average momentum fraction for each combination. Fixing the energy and coefficient spectrum of the ratio with the values extracted from the effective mass fits, we perform two-state fits as discussed above, to acquire the remaining four amplitudes, $\frac{\mathcal{A}^{\mu\nu}_{0,0}}{\sqrt{c_0(\vec{p})\, c_0(\vec{0})}}$, $\frac{\mathcal{A}^{\mu\nu}_{0,1}}{\mathcal{A}^{\mu\nu}_{0,0}}$, $\frac{\mathcal{A}^{\mu\nu}_{1,0}}{\mathcal{A}^{\mu\nu}_{0,0}}$, $\frac{\mathcal{A}^{\mu\nu}_{1,1}}{\mathcal{A}^{\mu\nu}_{0,0}}$ stemming from the expansion of the three-point function to two states. We analyze the appropriate ratio for each ensemble independently, and extract the ground state matrix element per q^2.

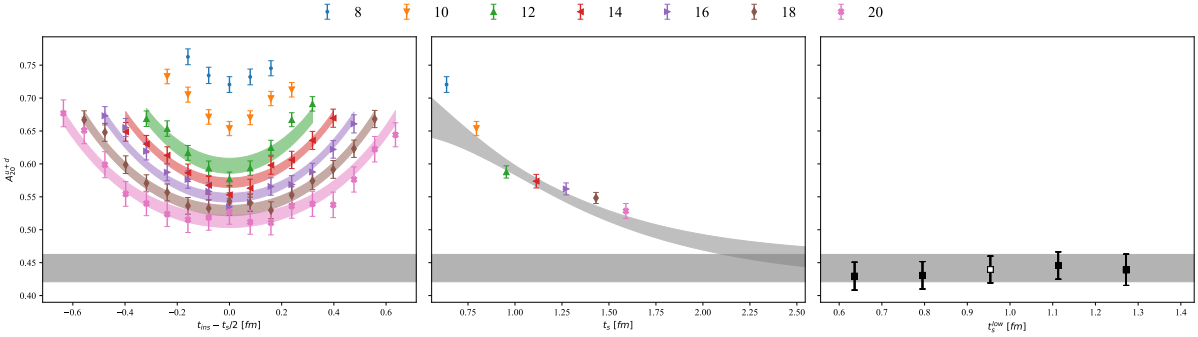

Figure 4: We show the excited state analysis of the renormalized ratio of Equation 4.14 for the isovector quantity of A_{20}, at zero momentum transfer, for the cB64 ensemble. Left panel: The ratio versus $t_{ins} - t_s/2$. The coloured bands are calculated using the two-state fits. Middle panel: The plateau values or middle points when no plateau can be identified, as a function of t_s. The gray band shows the predicted time-dependence of the ratio using the parameters extracted from the most probable two-state fit, at $t_{ins} = t_s/2$.Right panel: We show the values of the ground state matrix element as a function of t_s^{low}. The open symbol shows the most probable value, which is selected as the gray band spanning all three panels. In the header of the figure, we give the symbols used to denote the various t_s/a values.

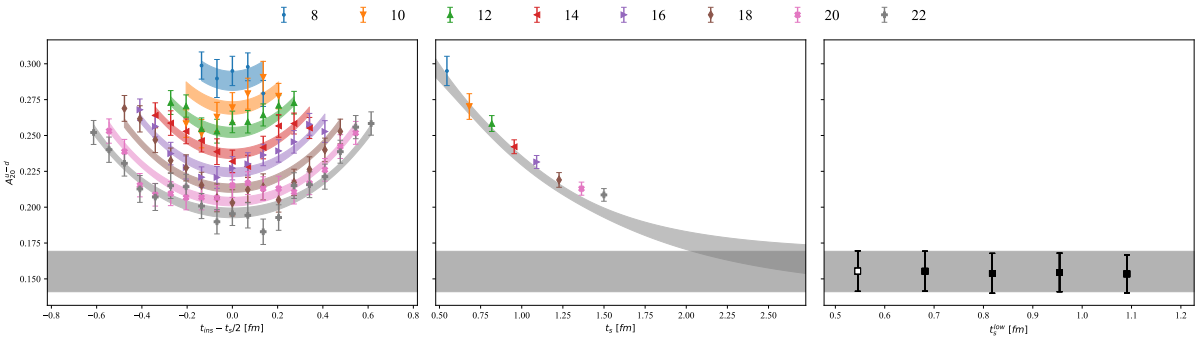

Figure 5: We show the excited state analysis of the renormalized ratio of Equation 4.14 for the isovector quantity of A_{20}, at zero momentum transfer, for the cC80 ensemble. The format and documentation of the panels is the same as in Figure 4.

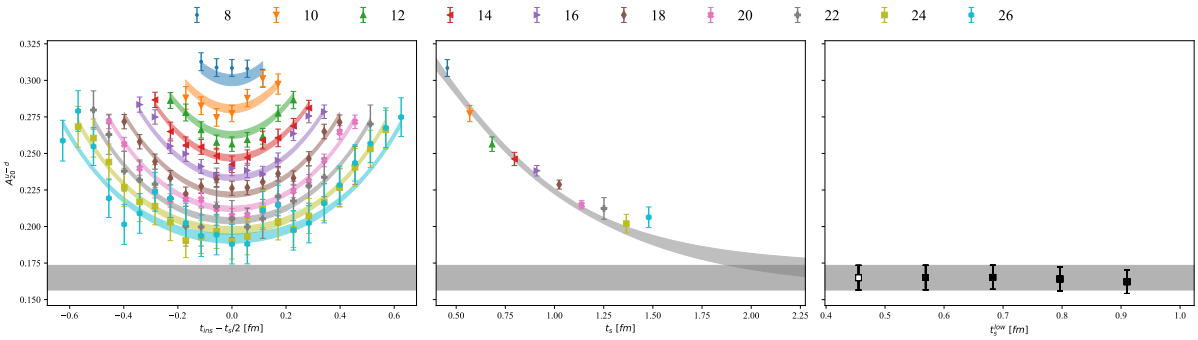

Figure 6: We show the excited state analysis of the renormalized ratio of Equation 4.14 for the isovector quantity of A_{20}, at zero momentum transfer, for the cD96 ensemble. The format and documentation of the panels is the same as in Figure 4.

4.4.3 Extracting the GFFs: $\mathbf{B_{20}}(Q^2)$

The value of B_{20} can be used alongside A_{20}, to calculate the nucleon angular momentum of quarks, as shown in Ref. [23]:

$$J = \frac{1}{2}\left(A_{20}(0) + B_{20}(0)\right) . \tag{4.27}$$

Unfortunately, for the case of B_{20}, as stated above, we are only able to derive its value at non-zero momentum transfer. Upon extracting the ground state matrix elements for several momentum transfers, we will later employ methods which will yield the necessary value, to compute the nucleon spin.

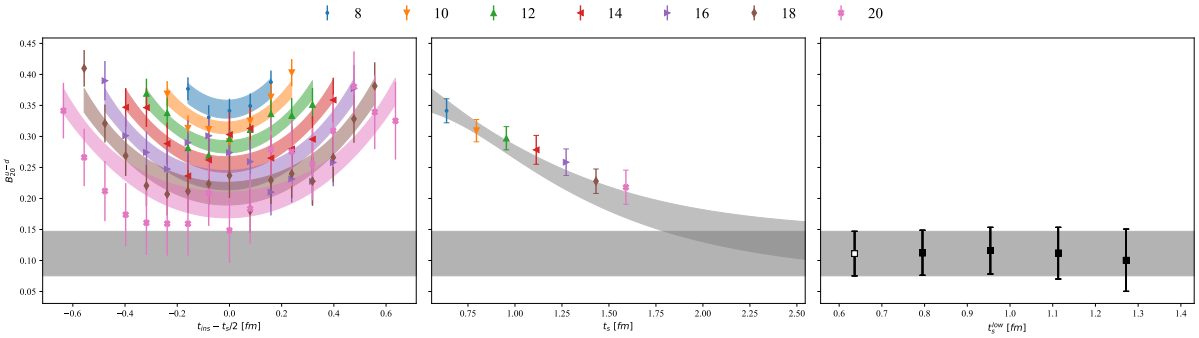

Figure 7: We show the excited state analysis of the renormalized ratio of Equation 4.14 for the isovector quantity of B_{20}, at momentum transfer 0.05GeV^2, for the cB64 ensemble. The format and documentation of the panels is the same as in Figure 4.

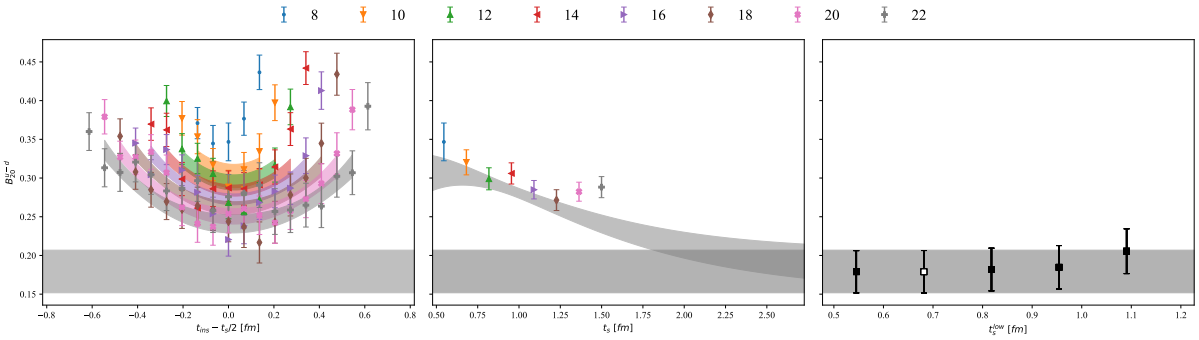

Figure 8: We show the excited state analysis of the renormalized ratio of Equation 4.14 for the isovector quantity of B_{20}, at momentum transfer 0.05GeV^2, for the cC80 ensemble. The format and documentation of the panels is the same as in Figure 4.

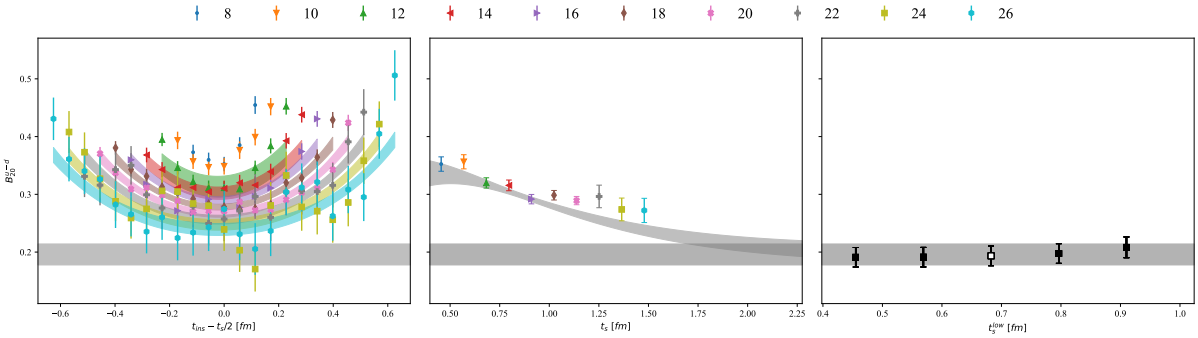

Figure 9: We show the excited state analysis of the renormalized ratio of Equation 4.14 for the isovector quantity of B_{20}, at momentum transfer 0.05GeV^2, for the cD96 ensemble. The format and documentation of the panels is the same as in Fig. 4.

4.5 Q^2-dependence of the generalized form factors (GFFs)

The Q^2 dependence of the nucleon matrix elements are modeled by a dipole Ansatz given by

$$F(Q^2) = \frac{F_0}{\left(1 + \frac{Q^2}{m^2}\right)^2}\,, \tag{4.28}$$

where $Q^2 = -(p'_\mu - p_\mu)^2$ is the Euclidean momentum transfer. To avoid inaccuracies coming from the extraction of the dipole mass parameter, we may make use of the relation between the slope of the form factor and the mean square radius, given by [24]:

$$\left\langle r^2 \right\rangle = -\frac{6}{F_0}\,\frac{\partial F(Q^2)}{\partial Q^2}\bigg|_{Q^2=0} = \frac{12}{m^2}\,. \tag{4.29}$$

The dipole Ansatz, then becomes

$$F(Q^2) = \frac{F_0}{\left(1 + \frac{Q^2}{12}\left\langle r^2 \right\rangle\right)^2}\,. \tag{4.30}$$

For some cases the Q^2-dependence is very mild for small Q^2 and the data become very noisy for larger values of Q^2. Such an example is B_{20}^{u+d}. In this case we fit only the small Q^2 region and expand the dipole to leading order in Q^2.

The fits to the Q^2-dependence for each ensemble is shown in Figs. 10 and 11 for isovector and isoscalar $A_{20}(Q^2)$ and $B_{20}(Q^2)$. As can be seen a dipole form provides a good description of the data. We give the results from the independent fits to each ensemble in the table that follows.

Table 5: Quantities obtained from the independent fits to each ensemble.

Ensemble	A_{20}^{u+d}		A_{20}^{u-d}		B_{20}^{u+d}	B_{20}^{u-d}	
	F_0	$\langle r^2\rangle$	F_0	$\langle r^2\rangle$	F_0	F_0	$\langle r^2\rangle$
cB64	0.401(22)	3.52(73)	0.170(11)	2.30(90)	-0.009(14)	0.133(26)	0.5(1.7)
cC80	0.365(27)	2.55(74)	0.152(12)	0.64(73)	-0.0057(82)	0.158(27)	2.7(1.6)
cD96	0.376(19)	2.92(54)	0.1568(78)	1.21(48)	0.0096(69)	0.198(17)	5.2(1.0)

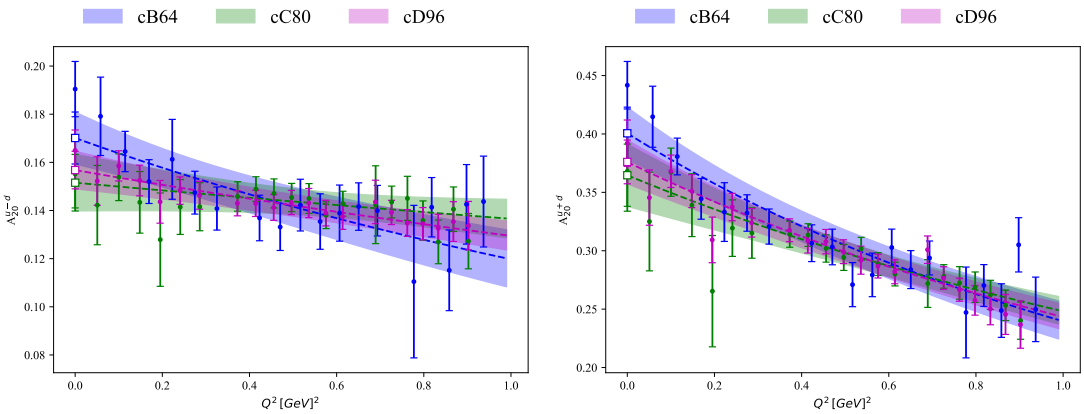

Figure 10: Preliminary results for the isovector (left) and connected isoscalar (right) GFF $A_{20}(Q^2)$ of the independent analysis for each ensemble.

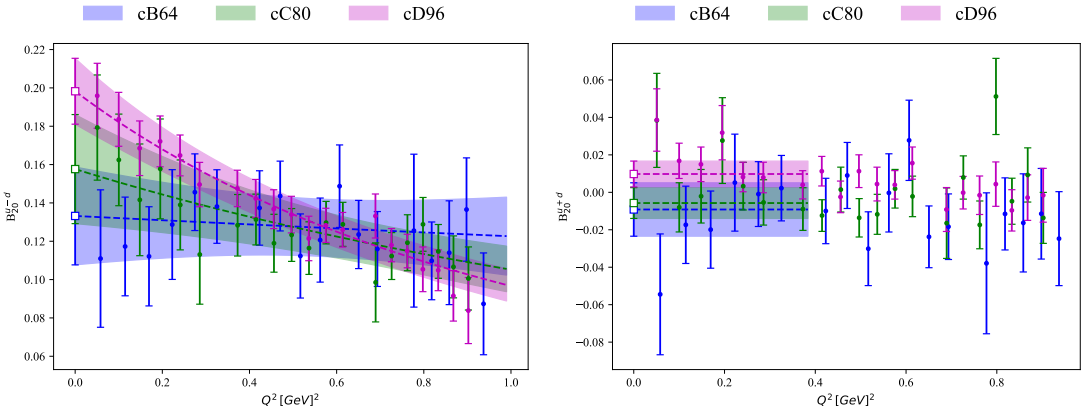

Figure 11: Preliminary results for the isovector (left) and connected isoscalar (right) GFF $B_{20}(Q^2)$ of the independent analysis for each ensemble.

4.6 Continuum limit

There are three ways to extrapolate our results to the continuum limit $\alpha \to 0$.

- First perform the Q^2 fits to the three ensembles separately and then extrapolate the two parameters of the dipole fits as a function of α^2, namely

$$\begin{aligned} F_0(\alpha^2) &= \bar{F}_0 + \alpha^2 F_2 \quad \text{and} \\ r^2(\alpha^2) &= r_0^2 + \alpha^2 r_2^2 \,. \end{aligned} \tag{4.31}$$

- A second approach would be interpolate the results of each ensemble at the *same* Q^2-value and find its continuum limit by a linear extrapolation in α^2. Then one can fit the the continuum extrapolated Q^2-dependence.

- A third approach is to simultaneously fit all three ensembles for Q^2 allowing α^2-dependent terms in the two parameters of the dipole fit. In this approach, one has to use a super-jackknife block of the three ensembles, as discussed in 3.2.2 and substitute Equation 4.31 to Equation 4.28 as follows

$$F(Q^2, \alpha^2) = \frac{\bar{F}_0 + \alpha^2 F_2}{\left(1 + \frac{Q^2}{12}(r_0^2 + \alpha^2 r_2^2)\right)^2} \,. \tag{4.32}$$

In this work we will use the third approach to determine the continuum limit.

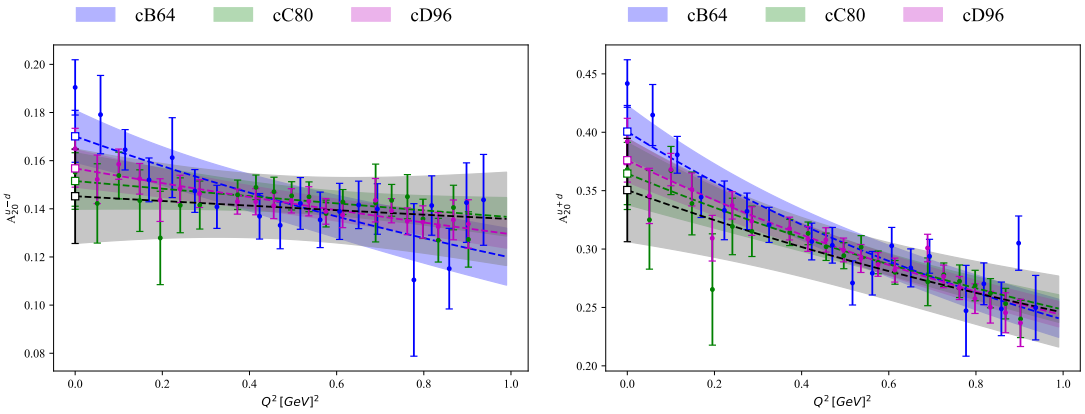

Figure 12: Preliminary results on the isovector (left) and connected isoscalar (right) GFF $A_{20}(Q^2)$ using superjackknife. The blue, green and pink curves show the behaviour of each ensemble per Q^2, using the parameters extracted from individual fits for each ensemble. The black curve is calculated using the parameters extracted from the simultaneous fit on all ensembles.

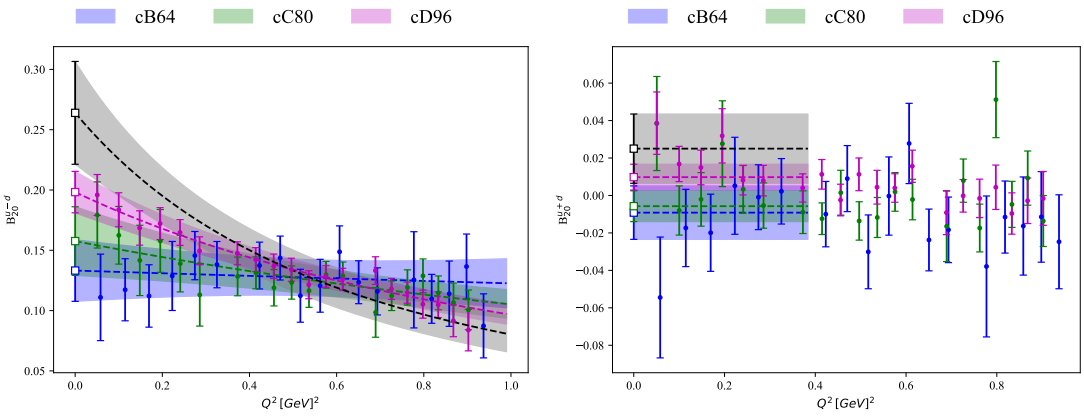

Figure 13: Preliminary results on the isovector (left) and connected isoscalar (right) GFF $B_{20}(Q^2)$ using superjackknife. The notation is the same as in Fig. 12.

For a better comparison, we tabulate our values of the extracted parameters for the isoscalar and isovector quantities of $A_{20}(0)$ and $B_{20}(0)$ in the table that follows.We proceed to compare our results with results from other studies.

Table 6: Extracted parameters from the universal analysis for the connected isoscalar and isovector quantities.

	A_{20}^{u+d}	A_{20}^{u-d}	B_{20}^{u+d}	B_{20}^{u-d}
F_0	0.351(44)	0.145(20)	0.025(18)	0.264(43)
$\langle r^2 \rangle$	2.3(1.3)	0.4(1.3)	-	9.8(2.8)

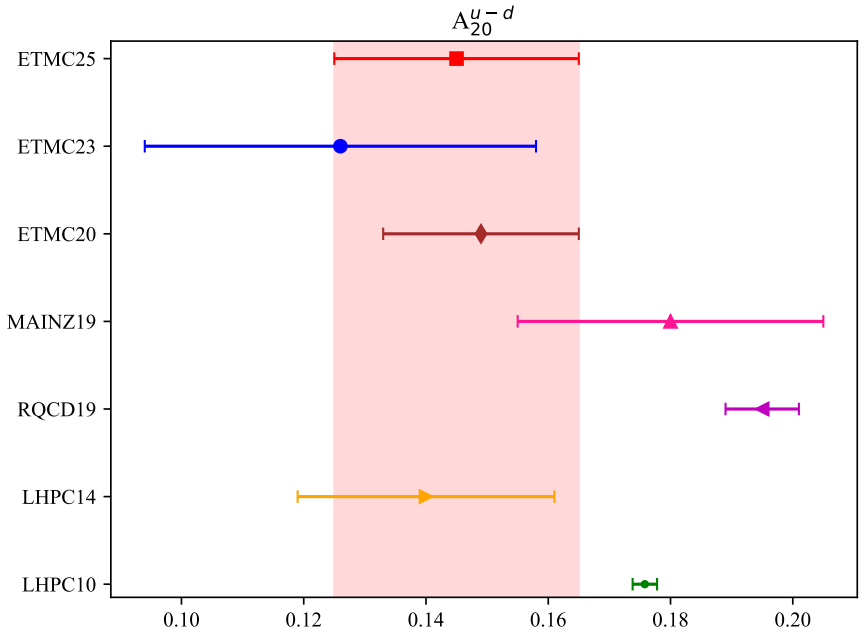

Figure 14: The results for A_{20}^{u-d} of this work compared with previous ETMC results [25],[26], the values from MAINZ19[27], RQCD19 [28], LHPC14 [29] and LHPC10[30].

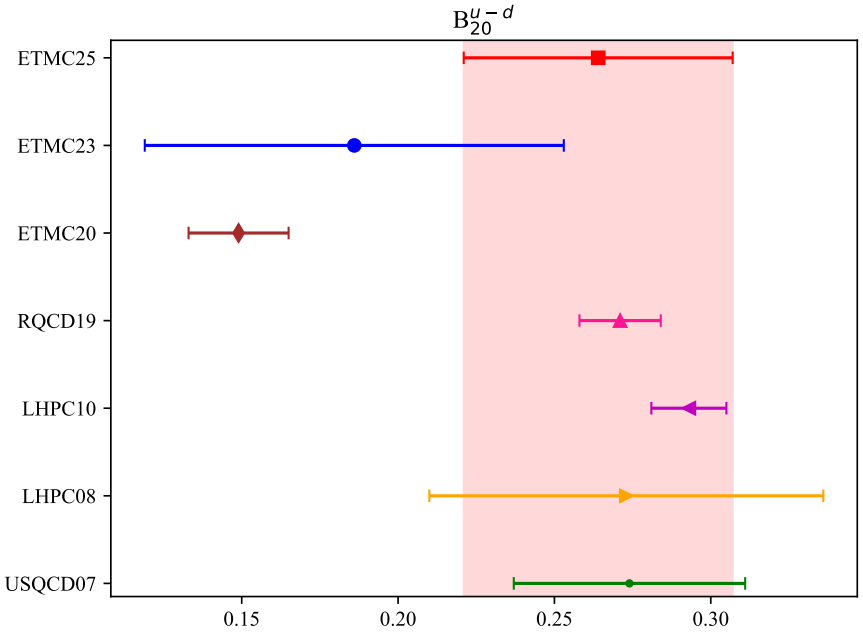

Figure 15: The results for B_{20}^{u-d} of this work compared with previous ETMC results [25],[26], the values from RQCD19 [28], ,LHPC10 [30], LHPC08 [31] and USQCD07 [32].

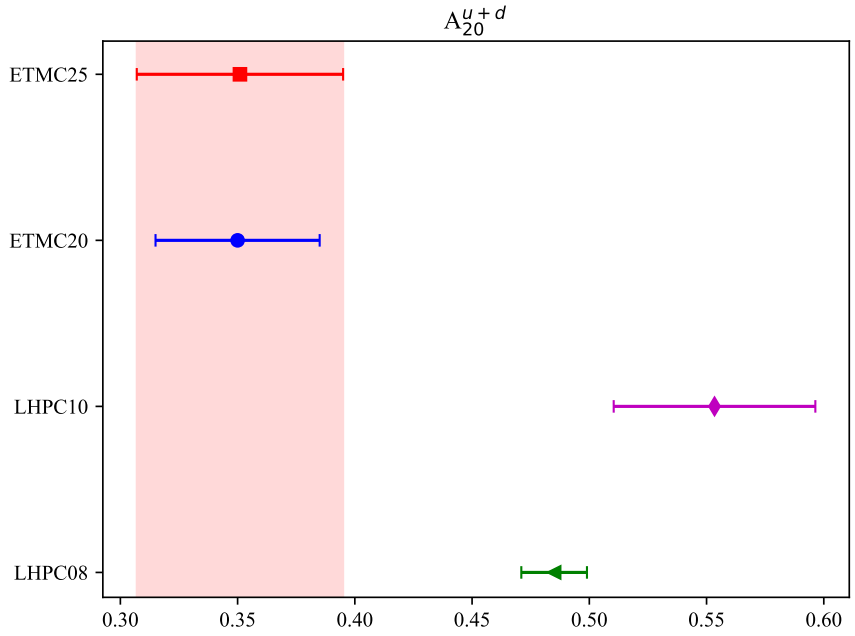

Figure 16: The results for connected A_{20}^{u+d} of this work compared with previous ETMC results [26], the values from LHPC10 [30] and LHPC08 [31].

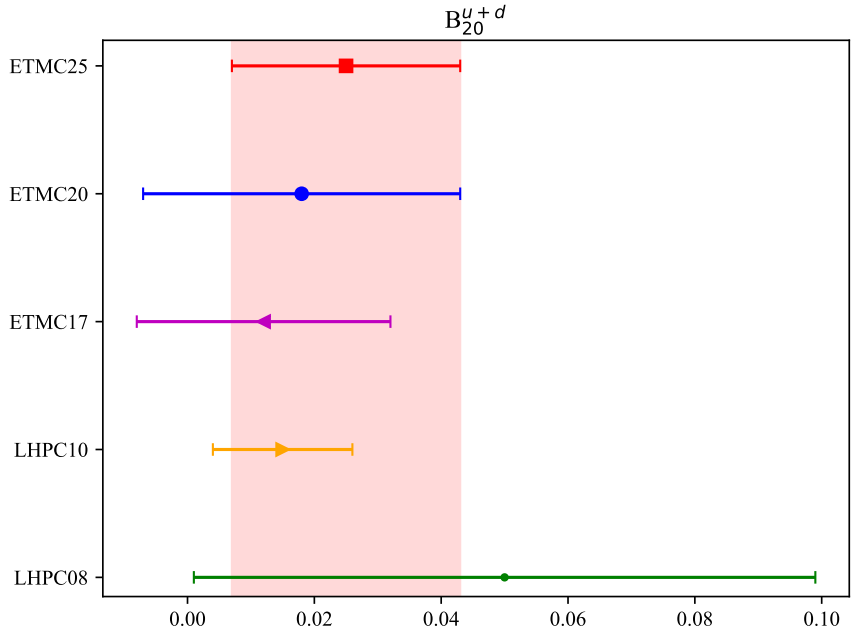

Figure 17: The results for connected B_{20}^{u+d} of this work compared with previous ETMC results [26],[33] the values from LHPC10[30] and LHPC08 [31].

5 Conclusions

In this thesis, we have given a calculation of the nucleon Generalised Form Factors $A_{20}(Q^2)$ and $B_{20}(Q^2)$, which at $Q^2 = 0$ can be used to extract the average momentum fraction and nucleon spin. We began by giving a brief introduction to the theory describing strong interactions, Quantum Chromodynamics, and discussed the discrete lattice formulation of it. Moving on, we gave the fundamental concepts for utilizing numerical methods in order to construct and analyze our data. Finally, we employed three $N_f = 2+1+1$ ensembles tuned to physical pion mass, to calculate the nucleon GFFs used to determine the average momentum fraction and nucleon spin and performed continuum limit extrapolations to extract their value as $\alpha \to 0$ using a method that combines all different ensembles into one universal fit.

To eliminate bias, we used model averaging and Akaike Information Criteria to obtain our final results. We have also employed the use of the generalized version of jackknife, known as super-jackknife, to be able to simultaneously analyze the three ensembles with different lattice spacings.

Finally, we have provided comparison between our results and multiple works for the isovector quantities we have computed. Since our values are in agreement with most cases, we conclude that the lattice approach can be a useful tool, providing reliable predictions for fundamental nucleon properties that could be difficult to measure otherwise.

A Basic properties of Hilbert spaces

A Hilbert space, $\mathcal{H}$ is a vector space, which is closed under vector addition and scalar multiplication. This means that, for any $|u\rangle$ and $|v\rangle \in \mathcal{H}$, and α, $\beta \in \mathbb{C}$, then

$$\alpha|u\rangle + \beta|v\rangle \in \mathcal{H}\,. \tag{A.1}$$

Apart from these, the inner product of two vectors in a Hilbert space produces a scalar, complex number. This result obeys the following two properties

$$\langle u|v\rangle = \langle v|u\rangle^*, \langle u|\alpha v + \beta w\rangle = \alpha\langle u|v\rangle + \beta\langle u|w\rangle\,, \tag{A.2}$$

where * denotes complex conjugation, $\alpha, \beta \in \mathbb{C}$ and $|u\rangle, |w\rangle, |v\rangle \in \mathcal{H}$ In the Hilbert spaces that interest us, have a set of linearly independent (basis) vectors ,such that any vector included in the Hilbert space can be written as a linear combination of the basis vectors. In that sense, the Hilbert spaces have a complete basis. A vector can be written as

$$|u\rangle = \sum_n \alpha_n |e_n\rangle\,, \tag{A.3}$$

where $|e_n\rangle$ is the nth basis vector, and α_n is in general a complex number. The basis is *orthonormal* if $\langle e_n|e_m\rangle = \delta_{nm}$ holds. We can also write the unit operator, $\mathbb{1}$ as a sum over the vectors of the complete orthonormal basis as

$$\mathbb{1} = \sum_n |e_n\rangle\langle e_n|\,. \tag{A.4}$$

When an operator $\widehat{O}$ acts on a vector in the Hilbert space, it maps it onto another vector, which is also a member of the space,

$$|v\rangle \in \mathcal{H} \Rightarrow \widehat{O}|v\rangle \in \mathcal{H}\,. \tag{A.5}$$

The adjoint operator, $\widehat{O}^\dagger$ is defined so that

$$\langle u|\widehat{O}|v\rangle = \langle u|\widehat{O}^\dagger|u\rangle^*\,. \tag{A.6}$$

If an operator is equal to its hermitian conjugate, $\widehat{O} = \widehat{O}^\dagger$ we call it hermitian or self-adjoint. In that case, its eigenvalues are real numbers and its eigenvectors are orthogonal, so if normalized, they become an orthonormal basis. Lastly, the trace of an operator is defined as

$$tr[\widehat{O}] = \sum_n \langle e_n|\widehat{O}|e_n\rangle\,, \tag{A.7}$$

where $|e_n\rangle$ are vectors of an orthonormal basis.

B SU(N) Lie groups and Lie algebra

B.1 Properties of the SU(N) group

The $SU(N)$ group consists of $N \times N$ complex, unitary matrices, with $\det[N] = 1$. It is closed under matrix multiplication, meaning that the product of any two members of the group is also a member of it. For example, for any two elements Ω_1, $\Omega_2 \in SU(N)$, such that $\Omega(x)_i^\dagger = \Omega(x)_i^{-1}$, and $\det[\Omega(x)_i] = 1$, then

$$\begin{gathered}(\Omega_1 \cdot \Omega_2)^\dagger = (\Omega_2^\dagger \cdot \Omega_1^\dagger) = (\Omega_2^{-1} \cdot \Omega_1^{-1}) = (\Omega_1 \cdot \Omega_2)^{-1} \quad \text{and} \\ \det[\Omega_1 \cdot \Omega_2] = \det[\Omega_1] \cdot \det[\Omega_2] = 1\end{gathered} \tag{B.1}$$

is also a member of the group. Since array multiplication is non-commutative, we call this in general, a *non-abelian group*.

B.2 Lie algebra

From the two main requirements for the members of the $SU(N)$ group, we conclude that $N^2 - 1$ real parameters are needed to describe these matrices. We can represent them by using basis matrices, T_j, known as generators, such that

$$\Omega = \exp\left(\mathrm{i} \sum_{j=1}^{N^2-1} \omega_j T_j\right), \quad \text{with } \omega_j \in \mathbb{R}\,. \tag{B.2}$$

Since Ω depend continuously on the parameters ω_j, the $SU(N)$ becomes a Lie group. Its generators, T_j are traceless, hermitian, complex $N \times N$ matrices that obey commutation and normalization conditions:

$$[T_j, T_k] = \mathrm{i}\, f_{jkl}\, T_l, \quad \mathrm{tr}[T_j T_k] = \frac{1}{2}\delta_{jk}\,. \tag{B.3}$$

The linear combinations between the parameters and generators of the group form the Lie algebra su(N). The elements of the algebra are complex $N \times N$ matrices, but they don't share the same properties as the group.

B.3 Generators of SU(2) and SU(3)

B.3.1 SU(2) generators

For SU(2) the generators are given by the Pauli σ-matrices:

$$T_j = \frac{1}{2}\sigma_j\,. \tag{B.4}$$

The anti-symmetric structure constant, f_{jkl} is taken as the Levi-Civita ϵ_{jkl} symbol.

B.3.2 SU(3) generators

For SU(3), the generators are given by the Gell-Mann λ-matrices, the 3×3 generalizations of the Pauli matrices:

$$T_j = \frac{1}{2}\lambda_j\,. \tag{B.5}$$

There are 8 λ-matrices, giving 8 different generators for the SU(3) group:

$$\begin{aligned}
\lambda_1 &= \begin{bmatrix} 0 & 1 & 0 \\ 1 & 0 & 0 \\ 0 & 0 & 0 \end{bmatrix}, \lambda_2 = \begin{bmatrix} 0 & \text{-i} & 0 \\ \text{i} & 0 & 0 \\ 0 & 0 & 0 \end{bmatrix}, \lambda_3 = \begin{bmatrix} 1 & 0 & 0 \\ 0 & -1 & 0 \\ 0 & 0 & 0 \end{bmatrix}, \\
\lambda_4 &= \begin{bmatrix} 0 & 0 & 1 \\ 0 & 0 & 0 \\ 1 & 0 & 0 \end{bmatrix}, \lambda_5 = \begin{bmatrix} 0 & 0 & \text{-i} \\ 0 & 0 & 0 \\ \text{i} & 0 & 0 \end{bmatrix}, \lambda_6 = \begin{bmatrix} 0 & 0 & 0 \\ 0 & 0 & 1 \\ 0 & 1 & 0 \end{bmatrix}, \\
\lambda_7 &= \begin{bmatrix} 0 & 0 & 0 \\ 0 & 0 & \text{-i} \\ 0 & \text{i} & 0 \end{bmatrix}, \lambda_8 = \frac{1}{\sqrt{3}} \begin{bmatrix} 1 & 0 & 0 \\ 0 & 1 & 0 \\ 0 & 0 & -2 \end{bmatrix}.
\end{aligned} \tag{B.6}$$

C Gamma Matrices

In Minkowski space, the 4×4 gamma matrices obey the anti-commutating relation

$$\{\gamma_\mu^M, \gamma_\nu^M\} = 2g_{\mu\nu}\mathbb{1}\,, \tag{C.1}$$

where the metric tensor is given by $g_{\mu\nu} = \text{diag}(1, -1, -1, -1)$. The gamma matrices in Euclidean space,γ_μ, with $\mu = 1, 2, 3, 4$ are related to the Minkowski gamma matrices, γ_μ^M, where $\mu = 0, 1, 2, 3$, by

$$\gamma_n = -\mathrm{i}\gamma_n^M, n = 1, 2, 3 \quad \text{and} \quad \gamma_4 = -\mathrm{i}\gamma_0^M\,. \tag{C.2}$$

The anti-commutating relation now is given by

$$\{\gamma_\mu, \gamma_\nu\} = 2\delta_{\mu\nu}\mathbb{1}\,. \tag{C.3}$$

As a result, $\gamma_\mu^2 = \mathbb{1}$. We also define the γ_5 matrix as the product

$$\gamma_5 = \gamma_1\gamma_2\gamma_3\gamma_4\,. \tag{C.4}$$

In addition, the gamma matrices are hermitian and unitary

$$\gamma_\mu = \gamma_\mu^\dagger = \gamma_\mu^{-1}, \quad \mu = 1, \cdots, 5\,. \tag{C.5}$$

The gamma matrices can be represented using the Pauli $2 \times 2\sigma$ matrices:

$$\gamma_{1,2,3} = \begin{bmatrix} 0 & -\mathrm{i}\sigma_{1,2,3} \\ \mathrm{i}\sigma_{1,2,3} & 0 \end{bmatrix}, \gamma_4 = \begin{bmatrix} 0 & \mathbb{1} \\ \mathbb{1} & 0 \end{bmatrix}, \gamma_5 = \begin{bmatrix} \mathbb{1} & 0 \\ 0 & -\mathbb{1} \end{bmatrix}\,. \tag{C.6}$$

D Kinematic factors for GFFs

We provide in Euclidean space the expressions of the GFFs and their kinematic factors, which are used for the SVD. In the expressions below, E_N is the nucleon energy for $\vec{q}$ for the case where $\vec{p}' = 0$. The kinematic factor $\mathcal{K} = \sqrt{2m_N^2/[E_N(E_N+m_N)]}$. Latin indices k,j and n take values 1,2,and 3, with $k \neq j$ while the Greek index ρ takes values 1,2,3, and 4. We note, however, that since in our analysis we use traceless data, Equation D.3 is taken to be 0.

$$\Pi^{00}(\Gamma^0,\vec{q}) = A_{20}\mathcal{K}\left(-\frac{3E_N}{8} - \frac{E_N^2}{4m_N} - \frac{m_N}{8}\right) + B_{20}\mathcal{K}\left(-\frac{E_N}{8} + \frac{E_N^3}{8m_N^2} + \frac{E_N^2}{16m_N} - \frac{m_N}{16}\right) + C_{20}\mathcal{K}\left(\frac{E_N}{2} - \frac{E_N^3}{2m_N^2} + \frac{E_N^2}{4m_N} - \frac{m_N}{4}\right), \tag{D.1}$$

$$\Pi^{00}(\Gamma^n,\vec{q}) = 0\,, \tag{D.2}$$

$$\Pi^{kk}(\Gamma^0,\vec{q}) = A_{20}\mathcal{K}\left(\frac{E_N}{8} + \frac{m_N}{8} + \frac{q_k^2}{4m_N}\right) + B_{20}\mathcal{K}\left(-\frac{E_N^2}{16m_N} + \frac{m_N}{16} - \frac{q_k^2E_N}{8m_N^2} + \frac{q_k^2}{8m_N}\right) + C_{20}\mathcal{K}\left(-\frac{E_N^2}{4m_N} + \frac{m_N}{4} + \frac{q_k^2E_N}{2m_N^2} + \frac{q_k^2}{2m_N}\right), \tag{D.3}$$

$$\Pi^{kk}(\Gamma^n,\vec{q}) = A_{20}\mathcal{K}\left(-i\frac{\epsilon_{kn0\rho}q_kq_\rho}{4m_N}\right) + B_{20}\mathcal{K}\left(-i\frac{\epsilon_{kn0\rho}}{4m_N}\right), \tag{D.4}$$

$$\Pi^{k0}(\Gamma^0,\vec{q}) = A_{20}\mathcal{K}\left(-i\frac{q_k}{4} - i\frac{q_kE_N}{4m_N}\right) + B_{20}\mathcal{K}\left(-i\frac{q_k}{8} + q\frac{q_kE_N^2}{8m_N^2}\right) + C_{20}\mathcal{K}\left(i\frac{q_k}{2} - i\frac{q_kE_N^2}{2m_N^2}\right), \tag{D.5}$$

$$\Pi^{k0}(\Gamma^n,\vec{q}) = A_{20}\mathcal{K}\left(-\epsilon_{kn0\rho}\left(\frac{q_\rho}{8} + \frac{q_\rho E_N}{8m_N}\right)\right) + B_{20}\mathcal{K}\left(-\epsilon_{kn0\rho}\left(\frac{q_\rho}{8} + \frac{q_\rho E_N}{8m_N}\right)\right), \tag{D.6}$$

$$\Pi^{kj}(\Gamma^0,\vec{q}) = A_{20}\mathcal{K}\frac{q_kq_j}{4m_N} + B_{20}\mathcal{K}\left(-\frac{q_kq_jE_N}{8m_N^2} + \frac{q_kq_j}{8m_N}\right) + C_{20}\mathcal{K}\left(\frac{q_kq_jE_N}{2m_N^2} + \frac{q_kq_j}{2m_N}\right), \tag{D.7}$$

$$\Pi^{kj}(\Gamma^n,\vec{q}) = A_{20}\mathcal{K}\left(-i\frac{\epsilon_{kn0\rho}q_kq_\rho}{8m_N} - i\frac{\epsilon_{jn0\rho}q_kq_\rho}{8m_N}\right) + B_{20}\mathcal{K}\left(-i\frac{\epsilon_{kn0\rho}q_kq_\rho}{8m_N} - i\frac{\epsilon_{jn0\rho}q_kq_\rho}{8m_N}\right). \tag{D.8}$$

List of Figures

List of Tables

References

[1] S. L. Glashow. Partial-symmetries of weak interactions. *Nuclear Physics*, 22(4):579–588, 1961. doi:10.1016/0029-5582(61)90469-2.

[2] S. Weinberg. A model of leptons. *Phys. Rev. Lett.*, 19:1264–1266, Nov 1967. doi:10.1103/PhysRevLett.19.1264.

[3] A. Salam. *Weak and electromagnetic interactions*, pages 244–254. doi:10.1142/9789812795915_0034.

[4] H. Fritzsch, M. Gell-Mann, and H. Leutwyler. Advantages of the color octet gluon picture. *Physics Letters B*, 47(4):365–368, 1973. URL: https://www.sciencedirect.com/science/article/pii/0370269373906254, doi:10.1016/0370-2693(73)90625-4.

[5] G. 't Hooft and M. Veltman. Regularization and renormalization of gauge fields. *Nuclear Physics B*, 44(1):189–213, 1972. URL: https://www.sciencedirect.com/science/article/pii/0550321372902799, doi:10.1016/0550-3213(72)90279-9.

[6] H. David Politzer. Reliable perturbative results for strong interactions? *Phys. Rev. Lett.*, 30:1346–1349, Jun 1973. doi:10.1103/PhysRevLett.30.1346.

[7] David J. Gross and Frank Wilczek. Asymptotically free gauge theories. i. *Phys. Rev. D*, 8:3633–3652, Nov 1973. doi:10.1103/PhysRevD.8.3633.

[8] Kenneth G. Wilson. Confinement of quarks. *Phys. Rev. D*, 10:2445–2459, Oct 1974. doi:10.1103/PhysRevD.10.2445.

[9] C. N. Yang and R. L. Mills. Conservation of isotopic spin and isotopic gauge invariance. *Phys. Rev.*, 96:191–195, Oct 1954. doi:10.1103/PhysRev.96.191.

[10] P. T. Matthews and A. Salam. The green's functions of quantised fields. *Il Nuovo Cimento (1943-1954)*, 12(4):563–565, 1954. doi:10.1007/BF02781302.

[11] P. T. Matthews and Abdus Salam. Propagators of quantized field. *Nuovo Cim.*, 2:120–134, 1955. doi:10.1007/BF02856011.

[12] Nicholas Metropolis, Arianna W. Rosenbluth, Marshall N. Rosenbluth, Augusta H. Teller, and Edward Teller. Equation of state calculations by fast computing machines. *The Journal of Chemical Physics*, 21(6):1087–1092, 06 1953. arXiv:https://pubs.aip.org/aip/jcp/article-pdf/21/6/1087/18802390/1087_1_online.pdf, doi:10.1063/1.1699114.

[13] J. D. Bratt, R. G. Edwards, M. Engelhardt, Ph. Hägler, H. W. Lin, M. F. Lin, H. B. Meyer, B. Musch, J. W. Negele, K. Orginos, A. V. Pochinsky, M. Procura, D. G. Richards, W. Schroers, and S. N. Syritsyn. Nucleon structure from mixed action calculations using 2+1 flavors of asqtad sea and domain wall valence fermions. *Physical Review D*, 82(9), November 2010. URL: http://dx.doi.org/10.1103/PhysRevD.82.094502, doi:10.1103/physrevd.82.094502.

[14] Christof Gattringer and Christian B. Lang. *Quantum chromodynamics on the lattice*, volume 788. Springer, Berlin, 2010. doi:10.1007/978-3-642-01850-3.

[15] Xiangdong Ji. Off-forward parton distributions. *Journal of Physics G: Nuclear and Particle Physics*, 24(7):1181–1205, July 1998. URL: http://dx.doi.org/10.1088/0954-3899/24/7/002, doi:10.1088/0954-3899/24/7/002.

[16] C. Alexandrou, S. Güsken, F. Jegerlehner, K. Schilling, and R. Sommer. The static approximation of heavy-light quark systems. a detailed lattice study. *Nuclear Physics B*, 414(3):815–855, 1994. URL: https://www.sciencedirect.com/science/article/pii/0550321394902623, doi:10.1016/0550-3213(94)90262-3.

[17] S. Gusken. A Study of smearing techniques for hadron correlation functions. *Nucl. Phys. B Proc. Suppl.*, 17:361–364, 1990. doi:10.1016/0920-5632(90)90273-W.

[18] G. W. Stewart. On the early history of the singular value decomposition. *SIAM Review*, 35(4):551–566, 1993. URL: http://www.jstor.org/stable/2132388.

[19] Constantia Alexandrou, Simone Bacchio, Martha Constantinou, Joseph Delmar, Jacob Finkenrath, Bartosz Kostrzewa, Marcus Petschlies, Luis Alberto Rodriguez Chacon, Gregoris Spanoudes, Fernanda Steffens, Carsten Urbach, and Urs Wenger. Quark and gluon momentum fractions in the pion and in the kaon. *Phys. Rev. Lett.*, 134:131902, Mar 2025. URL: https://link.aps.org/doi/10.1103/PhysRevLett.134.131902, doi:10.1103/PhysRevLett.134.131902.

[20] William I. Jay and Ethan T. Neil. Bayesian model averaging for analysis of lattice field theory results. *Physical Review D*, 103(11), June 2021. URL: http://dx.doi.org/10.1103/PhysRevD.103.114502, doi:10.1103/physrevd.103.114502.

[21] Ethan T. Neil and Jacob W. Sitison. Improved information criteria for bayesian model averaging in lattice field theory. *Physical Review D*, 109(1), January 2024. URL: http://dx.doi.org/10.1103/PhysRevD.109.014510, doi:10.1103/physrevd.109.014510.

[22] See Supplemental Material at http://link.aps.org/supplemental/10.1103/PhysRevLett.134.131902 for the details of the lattice simulation and of the renormalization procedure.

[23] Xiangdong Ji. Gauge-invariant decomposition of nucleon spin. *Physical Review Letters*, 78(4):610–613, January 1997. URL: http://dx.doi.org/10.1103/PhysRevLett.78.610, doi:10.1103/physrevlett.78.610.

[24] K. Goeke, J. Grabis, J. Ossmann, M. V. Polyakov, P. Schweitzer, A. Silva, and D. Urbano. Nucleon form factors of the energy-momentum tensor in the chiral quark-soliton model. *Physical Review D*, 75(9), May 2007. URL: http://dx.doi.org/10.1103/PhysRevD.75.094021, doi:10.1103/physrevd.75.094021.

[25] C. Alexandrou, S. Bacchio, M. Constantinou, P. Dimopoulos, J. Finkenrath, R. Frezzotti, K. Hadjiyiannakou, K. Jansen, B. Kostrzewa, G. Koutsou, G. Spanoudes, and C. Urbach. Moments of the nucleon transverse quark spin densities using lattice qcd. *Physical Review D*, 107(5), March 2023. URL: http://dx.doi.org/10.1103/PhysRevD.107.054504, doi:10.1103/physrevd.107.054504.

[26] C. Alexandrou, S. Bacchio, M. Constantinou, J. Finkenrath, K. Hadjiyiannakou, K. Jansen, G. Koutsou, H. Panagopoulos, and G. Spanoudes. Complete flavor decomposition of the spin and momentum fraction of the proton using lattice qcd simulations at physical pion mass. *Physical Review D*, 101(9), May 2020. URL: http://dx.doi.org/10.1103/PhysRevD.101.094513, doi:10.1103/physrevd.101.094513.

[27] Tim Harris, Georg von Hippel, Parikshit Junnarkar, Harvey B. Meyer, Konstantin Ottnad, Jonas Wilhelm, Hartmut Wittig, and Linus Wrang. Nucleon isovector charges and twist-2 matrix elements with $N_f = 2 + 1$ dynamical wilson quarks. *Phys. Rev. D*, 100:034513, Aug 2019. URL: https://link.aps.org/doi/10.1103/PhysRevD.100.034513, doi:10.1103/PhysRevD.100.034513.

[28] Gunnar Bali, Sara Collins, Meinulf Göckeler, Rudolf Rödl, Andreas Schäfer, and André Sternbeck. Nucleon generalized form factors from two-flavor lattice qcd. *Phys. Rev. D*, 100:014507, Jul 2019. URL: https://link.aps.org/doi/10.1103/PhysRevD.100.014507, doi:10.1103/PhysRevD.100.014507.

[29] J.R. Green, M. Engelhardt, S. Krieg, J.W. Negele, A.V. Pochinsky, and S.N. Syritsyn. Nucleon structure from lattice qcd using a nearly physical pion mass. *Physics Letters B*, 734:290–295, June 2014. URL: http://dx.doi.org/10.1016/j.physletb.2014.05.075, doi:10.1016/j.physletb.2014.05.075.

[30] J. D. Bratt, R. G. Edwards, M. Engelhardt, Ph. Hägler, H. W. Lin, M. F. Lin, H. B. Meyer, B. Musch, J. W. Negele, K. Orginos, A. V. Pochinsky, M. Procura, D. G. Richards, W. Schroers, and S. N. Syritsyn. Nucleon structure from mixed action calculations using $2 + 1$ flavors of asqtad sea and domain wall valence fermions. *Phys. Rev. D*, 82:094502, Nov 2010. URL: https://link.aps.org/doi/10.1103/PhysRevD.82.094502, doi:10.1103/PhysRevD.82.094502.

[31] Ph. Hägler, W. Schroers, J. Bratt, J. W. Negele, A. V. Pochinsky, R. G. Edwards, D. G. Richards, M. Engelhardt, G. T. Fleming, B. Musch, K. Orginos, and D. B. Renner. Nucleon generalized parton distributions from full lattice qcd. *Physical Review D*, 77(9), May 2008. URL: http://dx.doi.org/10.1103/PhysRevD.77.094502, doi:10.1103/physrevd.77.094502.

[32] Ph. Hägler, W. Schroers, J. Bratt, R. G. Edwards, M. Engelhardt, G. T. Fleming, B. Musch, J. W. Negele, K. Orginos, A. V. Pochinsky, D. B. Renner, and D. G. Richards. Nucleon generalized parton distributions from full lattice qcd, 2008. URL: https://arxiv.org/abs/0705.4295, arXiv:0705.4295, doi:10.1103/PhysRevD.77.094502.

[33] C. Alexandrou, M. Constantinou, K. Hadjiyiannakou, K. Jansen, C. Kallidonis, G. Koutsou, A. Vaquero Avilés-Casco, and C. Wiese. Nucleon spin and momentum decomposition using lattice qcd simulations. *Phys. Rev. Lett.*, 119:142002, Oct 2017. URL: https://link.aps.org/doi/10.1103/PhysRevLett.119.142002, doi:10.1103/PhysRevLett.119.142002.